Journal of Fluids and Structures 17 (2003) 433–459

JOURNAL OF FLUIDS AND STRUCTURES

www.elsevier.nl/locate/jnlabr/yjfls

On the bifurcations of a rigid rotor response in squeeze-film dampers

J.I. Inayat-Hussain[1], H. Kanki, N.W. Mureithi*

Department of Mechanical Engineering, Faculty of Engineering, Kobe University, Rokkodai 1-1, Nada-ku, Kobe 657-8501, Japan

Received 1 August 2001; accepted 10 October 2002

Abstract

The effectiveness of squeeze-film dampers in controlling vibrations in rotating machinery may be limited by the nonlinear interactions between large rotor imbalance forces with fluid-film forces induced by dampers operating in cavitated conditions. From a practical point of view, the occurrence of nonsynchronous and chaotic motion in rotating machinery is undesirable and should be avoided as they introduce cyclic stresses in the rotor, which in turn may rapidly induce fatigue failure. The bifurcations in the response of a rigid rotor supported by cavitated squeeze-film dampers resulting from such interactions are presented in this paper. The effects of design and operating parameters, namely the bearing parameter (B), gravity parameter (W), spring parameter (S) and unbalance parameter (U), on the bifurcations of the rotor response are investigated. Spring parameter (S) values between 0 and 1 are considered. A spring parameter value of $S = 0$ represents the special case of dampers without centering springs. With the exception of the case $S = 1$, jump phenomena appeared to be a common bifurcation that occurred at certain combinations of B, W and U irrespective of the value of S. Period-doubling and secondary Hopf bifurcations which occurred for low values of S ($\leqslant 0.3$) were not observed for the higher values $S \geqslant 0.5$. For very low stiffness values ($S < 0.1$), a period-3 solution that formed a closed bifurcation curve consisting of a pair of saddle-nodes, was found. Period-doubling cascades of the period-1 and period-3 orbits, boundary crisis and type 3 intermittency are the routes to chaos for this system. This study also revealed that combination values of gravity and spring parameters although resulting in similar values of the static eccentricity ratio exhibited remarkably different bifurcation behavior. The possibility of bifurcation phenomena arising from the interactions between large rotor imbalance forces and fluid-film forces in cavitated dampers, occurring in industrial rotating machinery, cannot be de-emphasized.

1. Introduction

Vibration phenomena induced by interaction between the rotor and fluid motion in fluid-film type of bearings are often encountered in rotating machinery installations. Such fluid–structure interaction is highly nonlinear and often results in nonsynchronous vibration of the rotor, whereby the rotor whirls at a different frequency from its rotational speed. This class of vibration is particularly destructive since the difference in the frequency of the whirl and rotation results in alternating flexural stresses in the rotor, which may eventually cause it to fail due to fatigue. Nonsynchronous vibration can only be controlled by introducing additional external damping into the rotor system. This sought after

*Corresponding author. Division of Applied Mechanics, Ecole Polytechnique de Montréal, Montréal, Québec, Canada, H3C 2A7. Fax: +81-078-8036155.

E-mail addresses: jawaid.inayat-hussain@engsci.monash.edu.my (J.I. Inayat-Hussain), njuki@mech.kobe-u.ac.jp (N.W. Mureithi).

[1] Present address: School of Engineering and Science, Monash University Malaysia, 2 Jalan Kolej, Bandar Sunway, 46150 Petaling Jaya, Selangor Darul Ehsan, Malaysia.

0889-9746/03/$ - see front matter
doi:10.1016/S0889-9746(02)00146-9

Nomenclature

B	bearing parameter, $\frac{\mu RL^3}{m\omega c^3}$
c	damper radial clearance, m
C_B	geometric center of the damper
C_J	geometric center of the journal
e	instantaneous eccentric position of the journal geometric center with respect to the damper geometric center, m
e_0	static eccentric position of the journal geometric center with respect to the damper geometric center, m
F_{D_X}	oil-film force in X-direction, N
F_{D_Y}	oil-film force in Y-direction, N
F_r	oil-film force in radial direction, N
F_t	oil-film force in tangential direction, N
G	rotor center of mass
g	acceleration due to gravity, m/s^2
k	centering spring stiffness, N/m
L	damper length, m
m	half-mass of rotor, kg
P	pressure (gauge), N/m^2
R	damper radius, m
S	spring parameter, $\frac{\omega_n}{\omega}$
t	time, s
U	unbalance parameter, $\frac{u}{c}$
W	gravity parameter, $\frac{g}{\omega^2 c}$
x	nondimensional displacement of the geometric center of the journal in the X-direction, $\frac{\bar{x}}{c}$
$\bar{x}$	displacement of the geometric center of the journal in the X-direction, m
$\bar{x}_0$	static eccentric position of the journal in the X-direction, m
X_0	static eccentricity ratio of the journal in the X-direction, $\frac{\bar{x}_0}{c}$
u	eccentricity of rotor center of mass, m
y	nondimensional displacement of the geometric center of the journal in the Y-direction, $\frac{\bar{y}}{c}$
$\bar{y}$	displacement of the geometric center of the journal in the Y-direction, m
$\bar{y}_0$	static eccentric position of the journal in the Y-direction, m
Y_0	static eccentricity ratio of the journal in the Y-direction, $\frac{\bar{y}_0}{c}$
$\bar{z}$	position in the Z-direction of the damper, m
α	angular position of the line connecting the static eccentric position of the journal to the damper center measured anti-clockwise from the positive X-axis, rad
γ	instantaneous angular position of the journal geometric center with respect to its static eccentric position measured anti-clockwise from the positive X-axis, rad
ε	nondimensional eccentricity ratio, $\frac{e}{c}$
ε_0	nondimensional static eccentricity ratio, $\frac{e_0}{c}$
θ	angular coordinate measured from the position of maximum film thickness in the direction of rotor angular speed, rad
θ_1	angular position of the start of positive pressure region measured from θ in the direction of rotor angular speed, rad
μ	dynamic viscosity of lubricant, Ns/m^2
τ	nondimensional time, ωt

ϕ	angular position of the line connecting the instantaneous eccentric position of the journal geometric center to the damper geometric center measured anti-clockwise from the positive X-axis, rad
ω	rotor angular speed, rad/s
ω_n	natural frequency of centering spring–rotor system, $\frac{k}{m}$, rad/s
(.)	denotes differentiation with respect to t
($'$)	denotes differentiation with respect to τ
Reference frames($X-Y-Z$)	stationary rectangular coordinate system with origin at the damper geometric center
($r-t$)	rotating rectangular coordinate system with origin at the damper geometric center

external damping is usually provided by squeeze-film dampers, which is a type of fluid-film bearing. In its simplest form, the squeeze-film damper consists of an oil-filled annular cavity surrounding the outer race of a rolling element bearing or the bearing segment of a hydrodynamic bearing. The outer race of the bearing, which acts as the damper's journal, is prevented from rotating, but is allowed to describe whirl orbit motion around its equilibrium position. During operation, as the damper's journal moves due to the dynamic forces acting on the rotor, the oil is displaced to accommodate these motions. Hydrodynamic pressures are consequently generated. These hydrodynamic pressures exert fluid-film forces on the journal surface and provide for a mechanism to reduce rotor whirl response amplitude and to attenuate the transmitted rotor forces. Successful application of the squeeze-film dampers to reduce synchronous vibration response at critical speeds and to eliminate rotor instability problems in steam turbines has been demonstrated by Kanki et al. (1998) and Leader et al. (1995), among others. In spite of their successful applications, there are certain operating conditions that may limit the effectiveness of the squeeze-film dampers in controlling rotor vibrations. Such conditions arise when the dynamic forces due to large rotor imbalance interact with fluid-film forces induced by dampers operating in a cavitated condition. When the lubricant in a damper is cavitated, not only is the damping capacity reduced due to low lubricant availability, but also a cross-coupled damping force that acts like a spring to support the rotor in its orbit is also generated. The loss in damping in itself is not nonlinear, but it eventually causes an increase in the response amplitude, which in turn causes the cross-coupled damping force to increase. As the cross-coupled damping force is a nonlinear function of the amplitude of vibration, the loss of damping due to cavitation coupled with large rotor amplitudes due to imbalance may subsequently give rise to nonsynchronous vibrations. Classical lubrication theory based on the incompressible Reynold's equation, albeit being widely used at present, is however inadequate to predict the dynamic performance of squeeze-film dampers operating in cavitated conditions. Accurate modelling of cavitation in squeeze-film dampers therefore remains a challenging and important problem. Equally important is the theoretical understanding of the dynamic behavior of the rotor-squeeze-film damper system; in particular, the nonlinear interaction between rotor imbalance forces with fluid-film forces in cavitated squeeze-film dampers, which is the aim of this paper.

Whilst the application of these dampers in industrial type rotating machinery is usually of a retrofit nature, their utilization in aircraft gas turbine engines are inevitable as such engines are mounted on rolling element bearings, which are known to provide almost negligible damping to the system. There are two basic configurations in which the dampers can be employed in rotating machinery installation. These configurations, which are known as the dampers with centering springs and those without centering springs, differ in the way the rotor finds its position in the damper clearance circle. In the damper without centering spring, the journal which usually lies at the bottom of the clearance circle when the rotor is at rest, is lifted when sufficient lift force is generated during running conditions of the rotor. In the damper with centering spring, the journal is usually centered in the damper by a retainer spring. Typical installation of both damper configurations is exhibited in Fig. 1.

Although the squeeze-film damper is an inherently stable machine element, it is nevertheless important to emphasize here that in spite of its inherent stable feature, its operation at certain parameters may give rise to undesirable nonsynchronous vibration. Theoretical and experimental studies in the past have demonstrated that such nonsynchronous vibrations and other nonlinear behavior can adversely affect the effectiveness of these dampers to attenuate vibration. The primary cause of such vibrations is generally attributed to the mass unbalance in the rotor (Holmes and Sykes, 1996). A degree of rotor unbalance, within the specified permissible tolerance, is always present in rotating machinery. The magnitude of the mass unbalance may, however, increase due to in-service rotor erosion or due to a partial or an entire failure of a blade. Given the harsh environment in which some rotating machinery such as aero gas turbine engines operate, and other causes such as bird strikes, for example, the occurrence of these problems are not uncommon. The increase of mass unbalance by a factor of 10 to 100 times the permissible level can therefore occur in

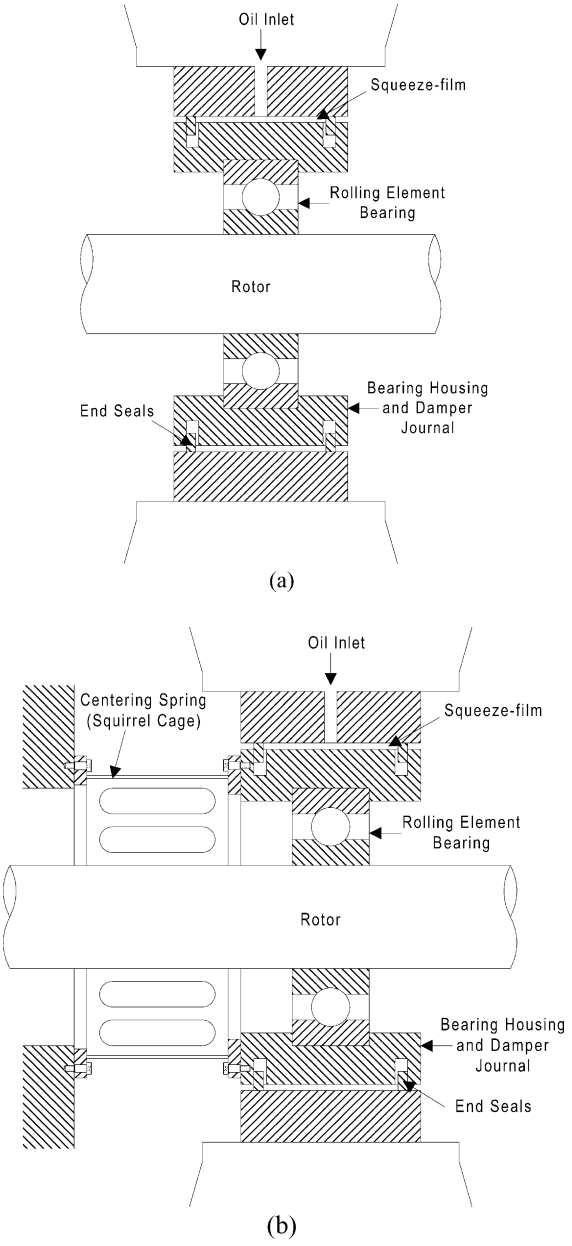

Fig. 1. Typical installation of a squeeze-film damper; (a) without centering springs; (b) with centering springs.

practice due to eroded rotors or in the event of a partial or an entire blade loss. It is therefore important to investigate the dynamic performance of the dampers to such abusive loading conditions. A brief review of available published work on the dynamic performance of squeeze-film dampers in rigid rotor applications follows.

The feasibility of supporting a rigid rotor in squeeze-film dampers without centering springs was theoretically investigated by Holmes (1972), utilizing a numerical integration scheme to solve the nonlinear equations describing the rotor motion in the damper. He further showed that a steady state orbit could not be achieved for low values of bearing parameter (B). The bearing parameter is a measure of the amount of damping that a squeeze-film damper can provide. It is a function of the length (L), diameter (D) and radial clearance (c) of the damper, the mass of the journal (m), lubricant viscosity (μ) and the operating speed of the rotor (ω). Physically, this means that sufficient lift of the journal is

not attained, and the journal merely rattles about in the clearance space of the damper in a never-ending transient. More importantly, the work showed that the damper produced a transmissibility of greater than unity, thus being ineffective in attenuating the forces to the machine supporting structure. The possibility of producing a transmissibility of less than unity for this type of damper was presented by Gunter et al. (1977) utilizing an essentially similar theoretical approach as adopted by Holmes (1972). For similar design and operating parameters, the transmissibility of this damper type was shown to be relatively large compared to that of a damper in parallel with centering springs. The damper without centering spring was also shown to produce a whirl orbit of period-2, mainly due to the unidirectional loading associated with the rotor weight acting on the oil-film. A modified cavitated short bearing theory, which accounted for the contribution of the negative pressure to the oil-film force, proposed by Humes and Holmes (1978) to predict the damper forces and subsequently the rotor response, compared relatively well with experimental measurements on a rotor test rig. This work theoretically showed that a rotor in uncavitated dampers without centering springs could not attain a steady state orbit. Cookson and Kossa (1979) theoretically investigated the influence of design and operating parameters that represent the rotor-damper system, on the rotor vibration response and damper attenuation capability. Their work showed that transmissibility of less than unity could be obtained for certain combinations of the gravity (W) and bearing (B) parameters. They further reported the occurrence of whirl orbits of period-2 and period-4 for certain parameter values. Experimental observations of nonlinear phenomena in experimental rigs representing aero-engine assemblies have been reported by Holmes and Dogan (1982) and Holmes and Dede (1989). In both references, a jump in the rotor orbital response was observed during run-up, indicating a softening spring effect associated with the damper induced fluid-stiffness forces. This was thought to be due to the entrainment of air into the damper thus changing the effective oil-film rupture condition. Recent work by Zeidan and Vance (1990) further confirmed the occurrence of jump phenomena of both the hardening and softening spring types in squeeze-film dampers. The hardening spring effect is associated with vapor cavitation which occurs when the dynamic pressure in the damper drops below the vapor pressure of the lubricant; whilst the softening spring effect is associated with gas cavitation due to entrainment of air into the damper.

The synchronous motion of a rigid rotor mounted on cavitated short squeeze-film dampers with linear centering springs has been thoroughly studied by Mohan and Hahn (1974). They obtained the steady state response of the rotor by assuming a circular centered whirl orbit and showed the existence of multiple valued responses characterizing a hardening spring system for considerably large values of unbalance. Taylor and Kumar (1980) have shown that the steady state response of a rigid rotor in uncavitated short squeeze-film dampers, assuming a circular centered whirl orbit, does not exhibit any nonlinear behavior. For the case of cavitated dampers, the results, similar to those of Mohan and Hahn (1974), showed the existence of jump phenomena for large unbalance magnitudes. Li and Taylor (1987) investigated the response of a rigid rotor on cavitated short squeeze-film dampers subjected to a unidirectional gravitational residual acting on the mass center of the journal, which resulted when the centering springs of the system did not perfectly balance the gravity load. The existence of quasi-periodic motion at certain parameters of the rotor system was observed for the case of a perfectly centered damper. They further showed that the static eccentricity due to the unidirectional gravitational residual transformed the quasi-periodic motion into synchronous or sub-synchronous motions. Zhao et al. (1994) employed the Floquet transition matrix method to examine the effect of eccentric cavitated short squeeze-film dampers on the stability of a rigid rotor. They observed that the periodic motion of the rotor, operating at a speed exceeding twice the system critical speed, with sufficiently large unbalance and static eccentricity, may lose its stability and bifurcate into sub-synchronous and quasi-periodic motions.

In the work presented herein, the numerical continuation scheme is employed to investigate the effect of cavitated squeeze-film dampers on the dynamic response of a rigid rotor. Unlike most of the previous published work on squeeze-film dampers, which treats the dampers with centering springs and those without centering springs separately, the nonlinear rotor response in both damper configurations are presented in this paper. A direct comparison of the response bifurcations in both damper configurations is possible due to the same range of parameters being used in this study for both damper cases. This task would otherwise be impossible from the previously published literature since different authors tend to use different ranges of design parameters. Of particular interest in this paper is the effect of centering spring stiffness on the response of the rotor. In a previous study, the authors had investigated the bifurcations of a rigid rotor response in cavitated squeeze-film dampers without centering springs (Inayat-Hussain et al., 2000). In this study, which is an extension of the previous one, the main object is to determine the bifurcations of the rotor response as the stiffness of the centering springs is progressively varied from zero, representative of dampers without centering springs, to relatively higher values that represent dampers with centering springs of various stiffness values. Numerical integration of the nonlinear equations is also undertaken in order to confirm the results of the continuation method, and also to seek for any aperiodic motion that might exist within the range of parameters investigated.

2. Formulation of the equations of motion

Theoretical oil-film forces in squeeze-film dampers are obtained by integrating the pressure distribution over the entire damper surface. The pressure distribution in the damper is obtained from the Reynolds equation, which is in turn derived from the Navier–Stokes equation by making the following simplifying assumptions (Szeri, 1980): (i) the oil-film thickness is small compared to the journal radius, therefore the curvature of the oil-film is negligible and the oil-film clearance can be developed out into a plane; (ii) the variation of pressure across the oil-film is small and can be neglected; (iii) the velocity component across the oil-film thickness (in the radial direction) is negligible compared to the flow in the axial and circumferential directions. Thus the flow of lubricant is two-dimensional; (iv) the lubricant flow is steady and therefore the inertial forces acting on a fluid element is negligible; (v) the body forces acting on a fluid particle are negligible; (vi) the flow of lubricant is laminar.

Closed-form analytical solutions for the Reynolds equation are available only for the extreme cases of either neglecting the pressure gradient in the circumferential direction or in the axial direction. The former is known as the short bearing approximation, whilst the latter as the long bearing approximation. Since most practical squeeze-film dampers have a ratio of length to diameter that is relatively small, typically between 0.2 and 0.3, they can be appropriately modelled based on the short bearing approximation. Fig. 2 shows the schematic of a rigid rotor in

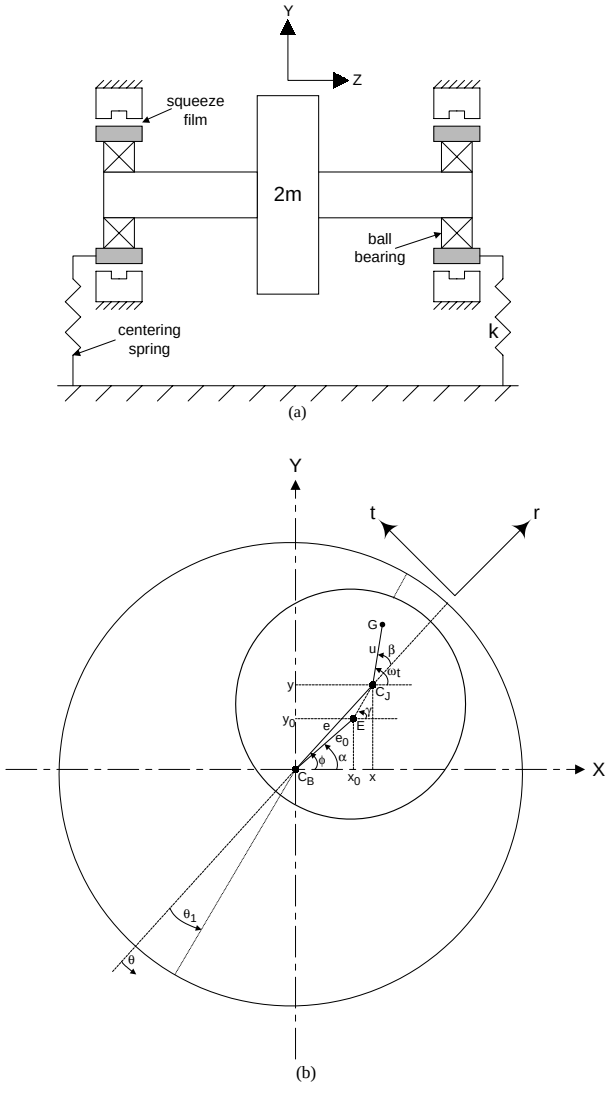

Fig. 2. (a) Schematic of a rigid rotor in squeeze-film dampers; (b) fixed and rotating coordinates systems.

squeeze-film dampers, and the fixed and rotating coordinate systems. The damper has no circumferential groove and its ends at $z = -L/2$ and $z = L/2$ are open. Most practical dampers are sealed at both ends, and a circumferential groove is commonly machined into the housing to ensure a continuous and uniformly distributed flow of oil through the damper's lands. For such damper design, the pressure profile generated by radial squeezing motion is equivalent to that for a damper without a circumferential groove and without end seals (Edney and Nicholas, 1999). The short bearing approximation has been successfully used to model practical squeeze-film dampers (Leader et al., 1995; Edney and Nicholas, 1999). The short bearing approximation is therefore adopted in this study. In the derivation of the oil-film forces, we further assume that the damper is cavitated. Cavitation is modelled based on the half-Sommerfeld boundary condition, which assumes the oil-film to extend over a length of π radians in the circumferential direction (Szeri, 1980). The contribution of the sub-ambient pressure to the oil-film forces is therefore neglected.

The pressure (P) distribution in a cavitated (π-film) short squeeze-film damper derived from the Reynold's equation is given in rotating coordinates as follows (Humes and Holmes, 1978):

$$P(\theta,\bar{z}) = \frac{6\mu}{c^2}\left(\bar{z}^2 - \frac{L^2}{4}\right)\frac{(\varepsilon\dot{\phi}\sin\theta + \dot{\varepsilon}\cos\theta)}{(1+\varepsilon\cos\theta)^3}, \tag{1}$$

where ε and $\dot{\varepsilon}$, respectively, denote the displacement and velocity in the radial direction, and $\dot{\phi}$ denotes the angular velocity. θ is the angular coordinate measured from the position of maximum film thickness in the direction of rotor angular speed, Fig. 2(b). L denotes the length of the damper, c the damper's radial clearance, $\bar{z}$ the position in the axial direction of the damper, and μ the dynamic viscosity of the lubricant. The resulting oil-film forces due to the motion of the journal in a squeeze-film damper are most conveniently expressed in polar coordinates. These forces are obtained by integrating the pressure distribution, given in Eq. (1), over the entire damper surface, and can be expressed as functions of $(\varepsilon,\dot{\varepsilon},\dot{\phi})$ as follows (Cookson and Kossa, 1979):

$$F_r = -\frac{\mu R L^3}{c^2}[I_1\dot{\varepsilon} + I_2\varepsilon\dot{\phi}], \quad F_t = -\frac{\mu R L^3}{c^2}[I_2\dot{\varepsilon} + I_3\varepsilon\dot{\phi}], \tag{2}$$

where F_r and F_t are the radial and tangential oil-film forces, respectively. Since cavitation is modelled based on the half-Sommerfeld boundary condition, the contribution of the negative pressure to the squeeze-film forces is neglected. The limits of integration of the pressure distribution in Eq. (1) are therefore determined so as to include only the positive pressure. From Eq. (1), the lubricant pressure is positive only when $\dot{\varepsilon}\cos\theta + \varepsilon\dot{\phi}\sin\theta < 0$. Therefore, the transition from positive pressure to negative pressure occurs when $\dot{\varepsilon}\cos\theta + \varepsilon\dot{\phi}\sin\theta = 0$. The limits of integration for a cavitated squeeze-film damper, assuming the half-Sommerfeld boundary condition is therefore between θ_1 and $\theta_1 + \pi$, where θ_1 denotes the angular position of the start of positive pressure region measured from θ. I_1, I_2, I_3 and θ_1 in Eq. (2) are therefore expressed as

$$\begin{aligned} I_1 &= \int_{\theta_1}^{\theta_1+\pi}\frac{\cos^2\theta}{(1+\varepsilon\cos\theta)^3}\,\mathrm{d}\theta, \quad I_2 = \int_{\theta_1}^{\theta_1+\pi}\frac{\sin\theta\cos\theta}{(1+\varepsilon\cos\theta)^3}\,\mathrm{d}\theta, \\ I_3 &= \int_{\theta_1}^{\theta_1+\pi}\frac{\sin^2\theta}{(1+\varepsilon\cos\theta)^3}\,\mathrm{d}\theta, \quad \theta_1 = \tan^{-1}\left(-\frac{\dot{\varepsilon}}{\varepsilon\dot{\phi}}\right). \end{aligned} \tag{3}$$

It is evident from the above equation that θ_1 is a function of the instantaneous nondimensional radial position (ε) and velocity ($\dot{\varepsilon}$), and the instantaneous nondimensional angular velocity ($\dot{\phi}$). The expressions of the integrals I_1, I_2 and I_3 have been previously evaluated analytically in closed form by Booker (1965). The closed form expressions are given below:

$$\begin{aligned} I_1 &= \left(-\frac{\varepsilon\sin\theta_1(3+(2-5\varepsilon^2)\cos^2\theta_1)}{(1-\varepsilon^2)^2(1-\varepsilon^2\cos^2\theta_1)^2} + \frac{\sigma(1+2\varepsilon^2)}{(1-\varepsilon^2)^{2.5}}\right), \\ I_2 &= \frac{2\varepsilon\cos^3\theta_1}{(1-\varepsilon^2\cos^2\theta_1)^2}, \\ I_3 &= \left(-\frac{\varepsilon\sin\theta_1(1-2\cos^2\theta_1+\varepsilon^2\cos^2\theta_1)}{(1-\varepsilon^2)(1-\varepsilon^2\cos^2\theta_1)^2} + \frac{\sigma}{(1-\varepsilon^2)^{1.5}}\right), \\ \sigma &= 0.5\pi - \tan^{-1}\left(\frac{\varepsilon\sin\theta_1}{(1-\varepsilon^2)^{0.5}}\right). \end{aligned} \tag{4}$$

The schematic of a rigid rotor in squeeze-film dampers is shown in Fig. 2(a). The rotor, which has a mass of $2m$, is mounted in two identical ball bearings, which are in turn supported by two squeeze-film dampers in parallel with centering springs. Each centering spring has a stiffness of k. The outer race of the ball bearing serves as the journal of the squeeze-film damper and is constrained from rotating by the centering spring assembly. In the case of squeeze-film

dampers without centering springs, mechanical linkages are used instead to prevent the journal from rotating. The purely static unbalance of the rotor is represented by the eccentricity (u) of its center of mass (G) from its geometric center of revolution, which in the case of the rigid rotor is identical to the geometric center of the journal, C_J. The notation and the coordinate frames used in the analysis of the rotor are shown in Fig. 2(b). The Cartesian coordinates (X, Y) are fixed in space and centered at C_B, the damper center. The polar coordinates (r, t) rotate at the whirl frequency of the journal in the damper. In the derivation of the equations of motion of a rigid rotor in squeeze-film dampers with centering springs, the following assumptions are made: (i) the rotor is rigid and symmetric; (ii) unbalance of the rotor is purely static and located in its midspan plane; (iii) gyroscopic effects are neglected; (iv) rotor motion in the axial direction is neglected; (v) the centering springs are linear; (vi) the rolling element bearings do not introduce significant excitation forces.

The first assumption implies that, throughout the operating speed range, the rotor behaves as a rigid body and does not deform. The assumption of the rotor being symmetric implies that the reactions at both dampers are equal. Lack of symmetry may either reflect the differences in the dynamic characteristics between the two dampers or axial offset of the mass center from the midspan of the rotor. The second assumption describes the condition of unbalance where the principal central inertia axis of the rotor is displaced parallel to its rotating center-line. The first four assumptions reduce the dynamics of the rotor to a two degrees of freedom model where only the translational motion in two orthogonal directions, namely X and Y, are considered. These assumptions further guarantee that the lowest natural mode of the rotor will be cylindrical, the first rigid body mode, where the motion of the journals in both dampers will be in-phase. This two degree of freedom model does not account for the existence of the conical mode of the rotor. The fifth assumption implies that the nonlinearity in the rotor system is attributed solely to the oil-film forces in the damper. With these assumptions being valid, it is sufficient to consider only one-half of the system. The motion of the system can be described by the displacements $\bar{x}$ and $\bar{y}$ of the geometric center of the journal from the center of the bearing housing. With the external forces acting on the journal that include the oil-film forces (F_{D_X} and F_{D_Y}), gravity, and unbalance forces, the equations of motion of the journal center become

$$\begin{aligned} m\ddot{\bar{x}} &= F_{D_X} - k\bar{x} + mu\omega^2 \cos \omega t, \\ m\ddot{\bar{y}} &= F_{D_Y} - k\bar{y} - mg + mu\omega^2 \sin \omega t. \end{aligned} \tag{5}$$

The oil-film forces, given in polar coordinates in Eq. (2), can easily be recast in Cartesian coordinates using the following equation:

$$\begin{aligned} F_{D_x} &= F_r \cos \phi - F_t \sin \phi, \\ F_{D_y} &= F_r \sin \phi + F_t \cos \phi. \end{aligned} \tag{6}$$

Inserting Eqs. (2) and (3) into Eq. (6), and the resulting equation into Eq. (5), and dividing the resulting equation by $m\omega^2 c$, and substituting the appropriate nondimensional parameters given in the nomenclature into the final equation, we obtain the following nondimensional governing equations for a rigid rotor mounted in cavitated squeeze-film dampers:

$$\begin{aligned} x'' &= -B\left[\frac{x}{\varepsilon}[I_1\varepsilon' + I_2\varepsilon\phi'] - \frac{y}{\varepsilon}[I_2\varepsilon' + I_3\varepsilon\phi']\right] \\ &\quad - S^2 x + U \cos \tau, \\ y'' &= -B\left[\frac{y}{\varepsilon}[I_1\varepsilon' + I_2\varepsilon\phi'] + \frac{x}{\varepsilon}[I_2\varepsilon' + I_3\varepsilon\phi']\right] \\ &\quad - S^2 y - W + U \sin \tau, \end{aligned} \tag{7}$$

where

$$B = \frac{\mu R L^3}{m\omega c^3}, \qquad S = \frac{\omega_n}{\omega}, \qquad U = \frac{u}{c}, \qquad W = \frac{g}{\omega^2 c}.$$

The bearing parameter (B) is a measure of the amount of damping that a squeeze-film damper can provide. The unbalance parameter (U), which is a measure of the rotor unbalance, is defined as the ratio of the eccentricity (u) of the rotor center of gravity (G) from its geometric center of rotation, to the radial clearance of the damper (c). The gravity parameter (W) represents the unidirectional static force acting on the damper. The spring parameter (S) is defined as the ratio of the undamped natural frequency of the centering spring–rotor system (ω_n) to the rotor angular speed (ω). τ is the nondimensional time. By setting the value of the spring parameter (S) to zero, Eq. (7) represents the case of a rigid rotor in squeeze-film dampers without centering springs; setting the gravity parameter (W) to zero, on the other hand, represents the case of a perfectly centered rigid rotor in squeeze-film dampers with centering springs. The case of nonzero S and W is representative of an eccentrically operated rigid rotor in squeeze-film dampers with centering

springs. The results presented in this paper are based on a range of parameters B between 0.015 and 0.15, W between 0 and 0.2, S between 0 and 5, and U between 0.05 and 0.8.

Eq. (7) is first transformed into a set of first-order ordinary differential equations and then solved using the numerical continuation method. The numerical continuation method, which determines how solutions of ordinary differential equations vary with the variation of a particular parameter, essentially traces a solution branch, detects bifurcation points and determines the stability of these points. It is further capable of switching from one solution branch to another, thus enabling the global solution structure of the system to be obtained. Computer programs for bifurcation analysis based on this method are currently available; one of such program, AUTO, described in Doedel et al. (1991a,b), is utilized in the work presented herein. A brief explanation on the algorithms implemented in AUTO and the basics of the continuation method follows.

The numerical continuation method has its foundation in function analysis. In the method, a bifurcation (or solution) branch is traced in parameter space, starting from a known solution (usually a fixed point or limit cycle). Consider the following first-order system:

$$\begin{aligned} &\dot{u}(t) = G(u(t), \lambda), \\ &u(.), G(.,.) \in R^n, \lambda \in R. \end{aligned} \tag{8}$$

A stationary solution (fixed point) will satisfy

$$\dot{u}(t) = G(u(t), \lambda) = 0, \qquad G(u(t), \lambda) : R^{n+1} \to R^n. \tag{9}$$

The solvability of Eq. (9) for the fixed-point solution curve $\dot{u} = u(\lambda)$ is guaranteed by the following Implicit Function Theorem.

Theorem. *Let $G(u, \lambda)$ be a continuously differentiable function in some open region containing the point (u_0, λ_0) such that $G(u_0, \lambda_0) = 0$, and Rank$[G_u^0 | G_\lambda^0] = n$; i.e., (u_0, λ_0) is a regular solution point. Then there exists $\alpha > 0$ and $\beta > 0$ such that* (i) *the equation $G(u, \lambda) = 0$ has a unique solution $u = u(\lambda)$ when $u_0 - \alpha < u < u_0 + \alpha$ and $\lambda_0 - \beta < \lambda < \lambda_0 + \beta$*; (ii) *the function $u(.)$ is continuously differentiable.*

To determine $u(\lambda)$ then, we start at a known solution (u_0, λ_0) of Eq. (9). Considering a continuation parameter (s) we have

$$G(u(s), \lambda(s)) = 0, \tag{10}$$

$$(u - u_0)^{\mathrm{T}} u_0' + (\lambda - \lambda_0)\lambda_0' - \Delta s = 0. \tag{11}$$

Eq. (11) defines a (pseudo) arc-length continuation condition on the (u, λ) plane. Note that $(\,)' = \mathrm{d}(\,)/\mathrm{d}s$

Newton's method is applied to Eqs. (10) and (11) leading to the following system at the kth step:

$$\begin{pmatrix} G_u^k & G_\lambda^k \\ u_0'\mathrm{T} & \lambda' \end{pmatrix} \begin{pmatrix} \Delta u^k \\ \Delta \lambda^k \end{pmatrix} = \begin{pmatrix} -G(u^k, \lambda^k) \\ \Delta s - (u^k - u_0)^{\mathrm{T}} u_0' - (\lambda^k - \lambda_0)\lambda_0' \end{pmatrix}, \tag{12}$$

$$u^{k+1} = u^k + \Delta u^k, \qquad \lambda^{k+1} = \lambda^k + \Delta \lambda^k.$$

Nonsingularity of the Jacobian in the system of Eqs. (10) and (11) marks a bifurcation point. At this singular point we have

$$N[G_u^0 | G_\lambda^0] = Span[\varphi_1, \varphi_2], \qquad N[G_u^0 | G_\lambda^0]^* = Span[\psi], \tag{13}$$

where '*' indicates the adjoint. A regularization procedure (essentially the Lyapunov–Schmidt procedure) is employed leading to the following extended system:

$$\begin{aligned} &G(x_0 + \alpha_1\varphi_1 + \alpha_2\varphi_2 + y) + \beta\psi = 0, \\ &y^{\mathrm{T}}\varphi_1 = 0, \\ &y^{\mathrm{T}}\varphi_2 = 0, \end{aligned} \tag{14}$$

where $x_0 = [u_0, \lambda_0]$. Solution of the resulting 'algebraic bifurcation equation' (Keller, 1991) gives the new solution directions. The bifurcating branches are

$$x_1 \approx x_0 + \alpha_1^1\varphi_1 + \alpha_2^1\varphi_2, \qquad x_2 \approx x_0 + \alpha_1^2\varphi_1 + \alpha_2^2\varphi_2. \tag{15}$$

The foregoing procedure can be extended to the more interesting case of determination of periodic solutions (limit cycles). The initial value problem

$$X' = f(X, \mu, t), \qquad X \in R^n, \mu \in R^{n_\mu} \tag{16}$$

is converted to the boundary value problem

$$\begin{aligned} &X'(\tau) = TF(X, \mu, \tau), \\ &X, F \in R^n, \quad \mu \in R^{n_\mu}, \quad \tau \in [0, 1], \end{aligned} \tag{17}$$

where T is the (unknown) period. The boundary value problem is numerically solved using orthogonal collocation with piecewise polynomial functions. A continuation and bifurcation analysis of this system yields both stable and unstable limit cycle solutions.

Clearly, only key elements of numerical continuation and bifurcation analysis have been highlighted. We refer the interested reader to Doedel et al. (1991a,b), Keller (1991) and Seydel (1988), and references therein for details.

Adaptive mesh strategies are employed in AUTO, which ensures solutions that are structurally correct. Detection of bifurcations is doubled checked using an eigenvalue analysis. For periodic solutions, Floquet multipliers are computed (one of the multipliers must be unity). Inaccuracies in the Floquet multipliers indicate poor algorithm convergence. The pseudo-arc length step size is a user-controlled parameter in AUTO, which can be adaptively varied to ensure optimum computational efficiency. Finally, results that remain questionable (at the minimum possible step size) can be verified by direct numerical simulation. Direct numerical integration of Eq. (7) is carried out using the MATLAB software package. This package utilizes a variable-step continuous solver based on an explicit Runge–Kutta (4,5) formula, the Dormand–Prince pair. It is a one-step solver, that is, in computing $x(t_n)$, it needs only the solution at the immediately preceding time point $x(t_{n-1})$.

3. Results and discussion

The dynamic response of the squeeze-film damper supported rotor is essentially governed by the four parameters B, S, W and U which have been previously defined. In the design of squeeze-film dampers for rotating machinery application, the gravity parameter (W) is first determined from the weight of the rotor, followed by the appropriate value of the spring parameter (S). The designer will then seek for the optimum value of the bearing parameter (B) that will ensure acceptable vibration response of the rotor for a range of likely unbalance parameter (U) values. The performance of squeeze-film dampers is usually measured in terms of the vibration response amplitude and the transmissibility. The transmissibility represents the damper's capability to attenuate the forces transmitted to the machine structure. It follows that the squeeze-film damper is effective if the transmissibility is less than unity, and ineffective if the transmissibility is greater than unity. A transmissibility equal to unity is representative of a rigidly supported rotor since all the applied forces are transmitted to the supporting structure. In this study, only the vibration response amplitude is considered to illustrate the bifurcations of the rotor response in the dampers. In the discussion of the results that ensues, the effect of the various parameters B, S, W and U on the bifurcations of the response will be first presented. Results of detailed bifurcation analysis for the case of the dampers without centering springs, and the case of eccentrically operated dampers with centering springs, will then be illustrated with the aim to highlight the role of the centering springs in modifying the bifurcation behavior of squeeze-film damper supported rotors. A brief explanation of the relationship between the spring parameter (S) and gravity parameter (W) in determining the static eccentricity ratio (Y_0) of the journal in the damper's clearance circle precedes the discussion of the results.

3.1. Relationship between the spring parameter (S), gravity parameter (W) and the static eccentricity ratio (Y_0)

The static eccentricity ratio (Y_0) is defined as the ratio of the static displacement of the journal in the Y-direction, $\bar{y}_0$, to the radial clearance of the damper, c. In this study, only the static eccentricity in the Y-direction is considered as precise centering-spring preload adjustment in this direction is usually not possible due to the effect of the gravitational force. Precise preload adjustment of the centering spring in the X-direction is, however, easily achieved. The relationship between the spring parameter (S), gravity parameter (W) and the static eccentricity ratio (Y_0) is given by

$$Y_0 = \frac{W}{S^2}, \tag{18}$$

This relationship is illustrated in Fig. 3 for a range of S values from 0.01 to 5 and for W values of 0.05, 0.1, 0.15 and 0.2. For $W = 0$, the equations of motion given in Eq. (7) represent a rigid rotor in perfectly centered squeeze-film

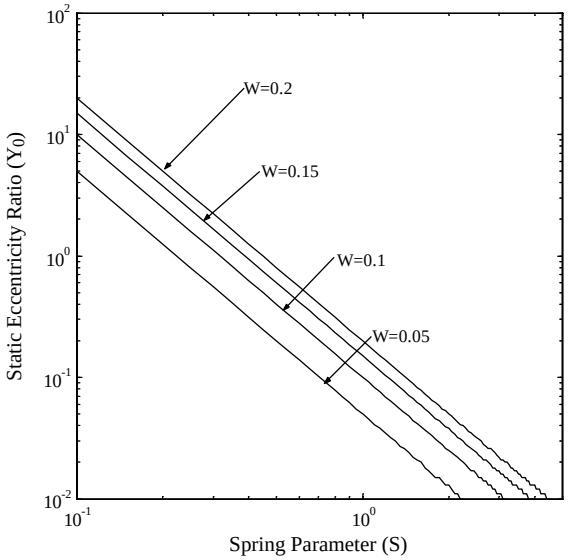

Fig. 3. Relationship between static eccentricity ratio (Y_0) and spring parameter (S) for various values of gravity parameter (W).

dampers with centering springs. For S value of zero, these equations represent a rigid rotor in squeeze-film dampers without centering springs. For the case of nonzero values of W and S, the equations are representative of a rigid rotor in eccentric squeeze-film dampers with centering springs. A combination of W and S values that results in Y_0 larger than 1 implies that the journal lies at the bottom of the clearance circle, similar to the case of dampers without centering springs. As the value of S becomes greater than 1, Y_0 approaches zero, representative of the perfectly centered damper with centering springs. In previous studies, the inverse of the spring parameter (S), which is known as the speed parameter, has often been used to investigate the response of a rotor in squeeze-film dampers with centering springs (Taylor and Kumar, 1980; Li and Taylor, 1987; Zhao et al., 1994). Gunter et al. (1977) showed that, for the operation of squeeze-film dampers at an equivalent value of S greater than 0.7071, the transmissibility will exceed unity regardless of the value of unbalance parameter, thus rendering it ineffective in this range of S. The values of the gravity parameter (W) for squeeze-film dampers employed in some aero gas turbine engines were determined by Cookson and Kossa (1979) to be in the range of 0.008–0.222. The values of W between 0.0 and 0.2 and S between 0.0 and 1, utilized in this study, are believed to cover the range of practical interest.

3.2. *Effect of bearing parameter (B)*

The bearing parameter (B), as previously defined, is a measure of the damping capacity of the squeeze-film damper. It is dependent on the length (L), diameter (D) and radial clearance (c) of the damper, the mass of the journal (m), lubricant viscosity (μ) and the operating speed of the rotor (ω). Whilst the design parameters L, D, c and m are fixed, the viscosity (μ) may vary due to temperature increase in the damper during operation, thus affecting the value of the bearing parameter (B). Since it is not possible to exactly define a range of practical B values due to its dependency on various parameters, we have conveniently chosen B values of 0.015, 0.05, 0.1 and 0.15. As will be shown shortly, these values appropriately represent both the cases of dampers with low and high damping capacity. Fig. 4 shows the effect of these B values on the response of the rotor with the variation of spring parameter (S). The value of U is 0.05, and the response of the rotor is illustrated for W values of 0.0, 0.05, 0.1 and 0.2. In this figure, and other figures that follow suit, stable solutions are shown as continuous curves, while the unstable solutions are indicated by segmented lines. The solution curves in Fig. 4 are all of period-1. The peaking of the response at $S = 1$ is due to resonance when the operating speed is equal to the natural frequency of the rotor-centering spring system. It is in this region that the role of B is most significant. As obvious from the response curves shown in Fig. 4, increasing B reduces the response amplitude at resonance. As the value of W is increased from 0.0 to 0.2, increasing the value of B is also found to decrease the response amplitude in the range of S less than 1. It is further observed that saddle-node bifurcations, denoted by ☆ in Fig. 4, occur for values of $B = 0.015$ and $W = 0.0$, 0.05 and 0.1. Whilst it is admitted that the results shown in Fig. 4 do not give the entire picture of the effect of B on the bifurcations of the rotor response due to the relatively small value of U, which may have not been sufficient to cause the rotor to lose its stability, the results nevertheless point to the fact

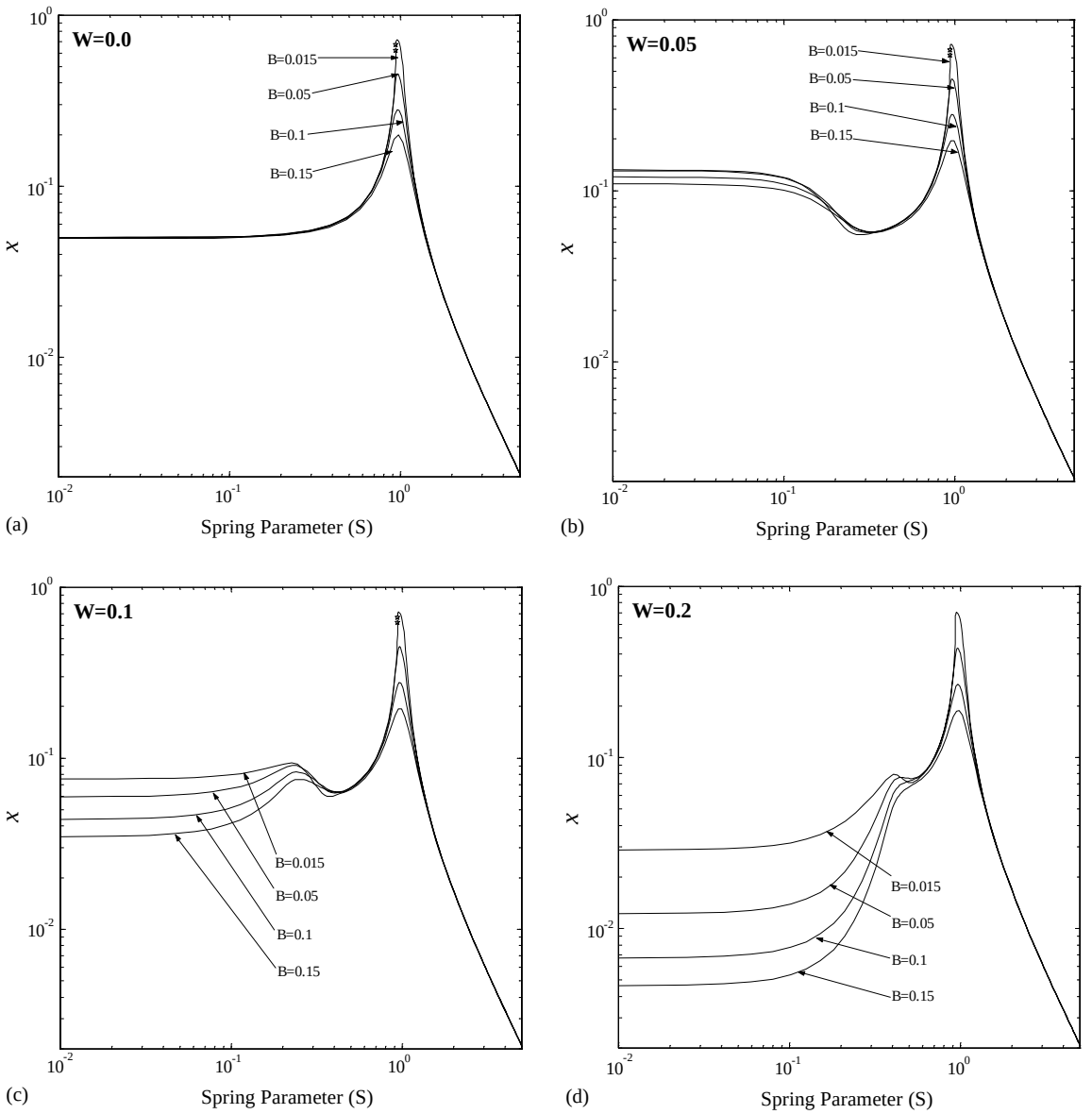

Fig. 4. Effect of bearing parameter (B) on the rotor response for unbalance parameter (U) of 0.05 and gravity parameter (W) of (a) 0.0; (b) 0.05; (c) 0.1; (d) 0.2. Bifurcation is: ☆ saddle-node.

that relatively high values of B suppress the bifurcations of the response, and for the case of low B values, the bifurcations cease to occur when W is increased. The effect of U on the bifurcation behavior is discussed next.

3.3. *Effect of unbalance parameter (U)*

The effect of the unbalance parameter (U) on the vibration response of the rotor with the variation of the spring parameter (S) is shown in Fig. 5. The value of B is 0.015, the values of U are 0.05, 0.1, 0.2 and 0.3, and the response of the rotor is shown for values of W of 0.0, 0.05, 0.1 and 0.2. The solution curves in Fig. 5 are all of period-1. For all values of W, saddle-node bifurcations are found to occur as the value of the spring parameter approaches 1. The saddle-node bifurcation, which causes a sudden increase in the rotor response amplitude when a certain value of S is reached, is also known as the jump phenomenon. The jump phenomenon in Fig. 5 is characteristic of a hardening spring since a

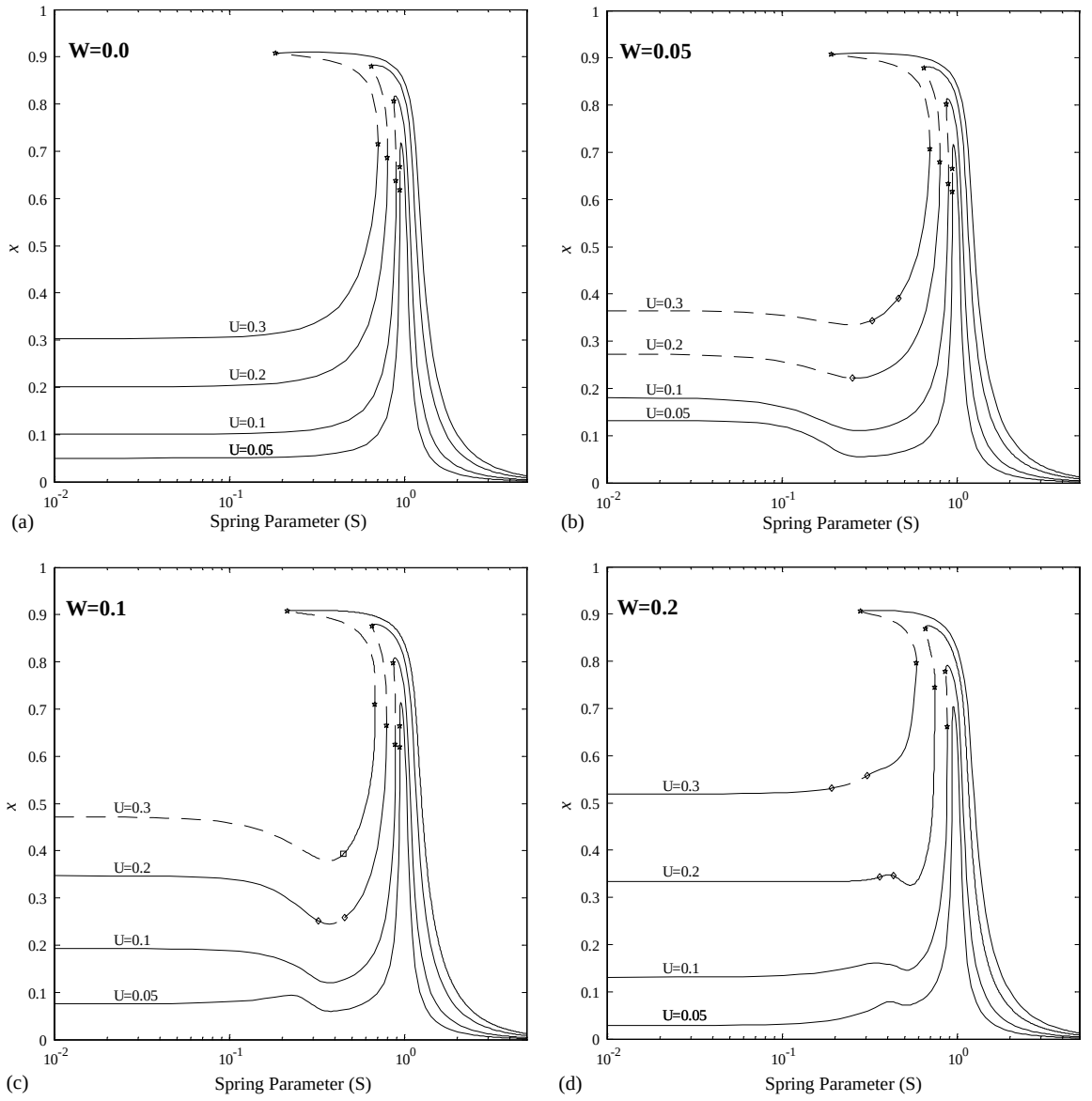

Fig. 5. Effect of unbalance parameter (U) on the rotor response for bearing parameter (B) of 0.015 and gravity parameter (W) of (a) 0.0; (b) 0.05; (c) 0.1; (d) 0.2. Bifurcations are: ☆ saddle-node; ◇ period-doubling; □ secondary Hopf.

jump down in the response occurred on run-up of the rotor, i.e., decreasing S (Holmes and Box, 1992). Increase in the unbalance parameter (U) not only increases the response amplitude, but also causes the spring parameter (S) values where these phenomena occur to decrease. It is further observed that when the gravity parameter (W) is nonzero, period-doubling bifurcations, denoted by ◇ in Fig. 5, occurred for higher values of U, namely, 0.2 and 0.3. For the case of $W = 0.05$, the response is unstable prior to the period-doubling bifurcation for values of S smaller than the critical value at the bifurcation point. For the case of $W = 0.1$, a secondary Hopf bifurcation, denoted by γ in Fig. 5(c), is observed to occur for the case of $W = 0.3$. Below the value of the critical spring parameter (S) where the bifurcation occurs, the response is unstable. The secondary Hopf bifurcation is only observed to occur for the case of $W = 0.1$. For the case of $W = 0.2$, which also revealed the occurrence of period-doubling bifurcation, the response below the critical value of S where the bifurcation occurs is, however, stable. This is also observed for the case of $U = 0.2$ and $W = 0.1$. To have a general appreciation of the allowable unbalance parameter (U) magnitude in practical rotating machinery, the ISO 1940 (1973) is referred to. According to the ISO 1940, the balance quality of rigid turbo-generator rotors,

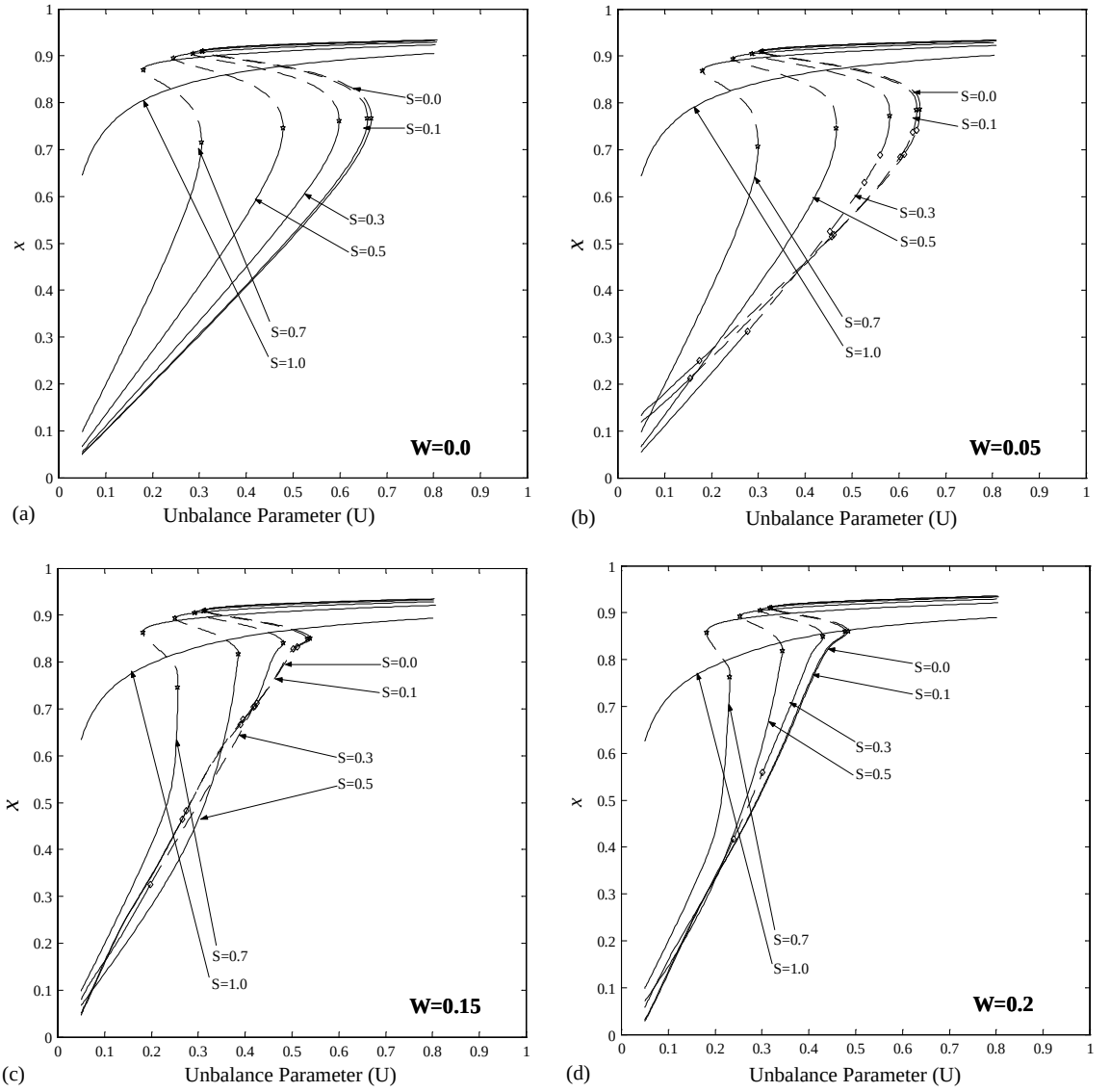

Fig. 6. Effect of spring parameter (S) on the response of the rotor to imbalance for bearing parameter (B) of $=0.015$ and gravity parameter (W) of (a) 0.0; (b) 0.05; (c) 0.15; (d) 0.2. Bifurcations are: ☆ saddle-node; ◇ period-doubling.

turbo-compressors, gas and steam turbines are classified under grade G2.5. For a maximum operating speed of 10 000 r.p.m., the G2.5 specifies the permissible eccentricity of the rotor mass center from its geometric center (u) of 2.5 μm. For a typical squeeze-film damper in aero gas turbine engine application, which has a radial clearance (c) of 100 μm, the permissible unbalance parameter (U) is therefore 0.025 (Gunter et al., 1977). The values of U where bifurcations of the rotor occurred, as seen in Fig. 5, are only about one order of magnitude higher than the permissible level, and can be achieved due to in-service rotor erosion or in the event of a partial or an entire blade failure (Inayat-Hussain, 2001).

3.4. Effects of spring (S) and gravity (W) parameters

Fig. 6 shows the bifurcation diagram exhibiting the variation of the rotor response amplitude as the unbalance parameter (U) is varied from 0.0 to 0.8 for spring parameter values (S) of 0.0, 0.1, 0.3, 0.5, 0.7 and 1.0. The bearing parameter (B) is fixed at 0.015, and plots for various W values of 0.0, 0.05, 0.15 and 0.2 are given in Fig. 6. The solution

curves in Fig. 6 are all of period-1. The limiting case $S = 0.0$, $W = 0.0$ represents a perfectly centered rigid rotor in squeeze-film dampers without centering springs. This limiting case is physically representative of a vertical rigid rotor centered in squeeze-film dampers without centering springs ($S = 0.0$); in this case the effect of gravitational force on the rotor is negligible ($W = 0.0$). The response curves for the case of $S = 0.0$ and 0.1 are found to be quite similar suggesting that the dynamics of both cases are the same. The combination values of $S = 0.1$ and W values of either 0.05, 0.1, 0.15 or 0.2 result in a static eccentricity ratio greater than 1, implying that the journal is initially in contact with the damper's clearance circle limit. The similarity observed in the dynamics of the rotor in the dampers with spring parameter (S) of 0.1 with that of the damper without centering springs is attributed to the low stiffness of the centering spring, whose magnitude is negligible compared to the stiffness generated by the oil-film radial force. For the case of $W = 0.0$, only the saddle-node bifurcation occurs. For the case of $W = 0.05$, 0.1 and 0.15, period-doubling bifurcations are found to precede the saddle-node bifurcations for the lower values of S, namely 0.0, 0.1 and 0.3. For the case of $W = 0.1$ in particular, the secondary Hopf bifurcation is found to occur preceding the period-doubling bifurcation.

In order to have a physical appreciation of the motion of the rotor in the damper, rotor whirl orbit plots are exhibited in Fig. 7. The rotor whirl orbits are all stable period-1 solutions computed using the numerical integration scheme. The rotor whirl orbits, which represent the instantaneous position of the journal in the damper clearance circle, illustrate the influence of the spring parameter (S) on the response amplitude of the rotor. The value of the bearing parameter (B) is 0.015 and the gravity parameter W is 0.05. This figure clearly illustrates the whirl orbits change from a noncircular shape to a circular shape as the spring parameter (S) is increased from 0.0 to 1.0. For low values of S, the orbits whirl at

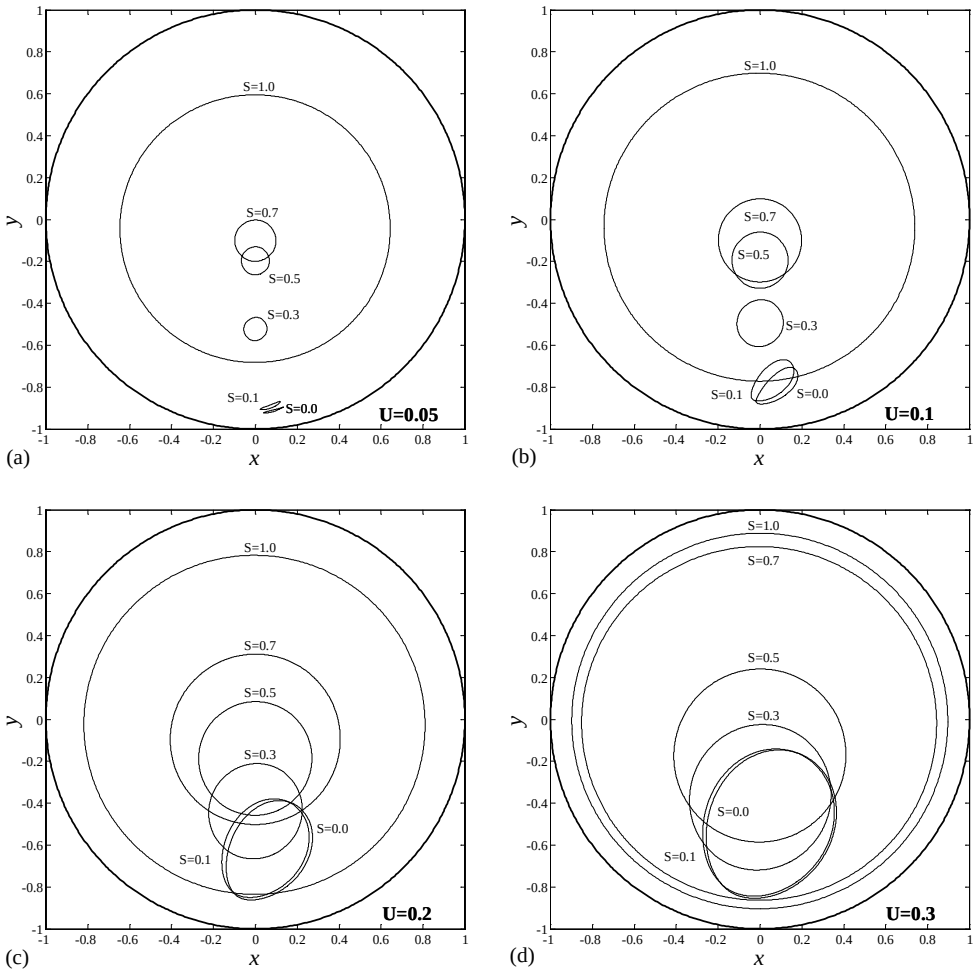

Fig. 7. Effect of spring parameter (S) on the rotor whirl orbit response for bearing parameter (B) of 0.015, gravity parameter (W) of 0.05 and unbalance parameter (U) of (a) 0.05; (b) 0.1; (c) 0.2; (d) 0.3.

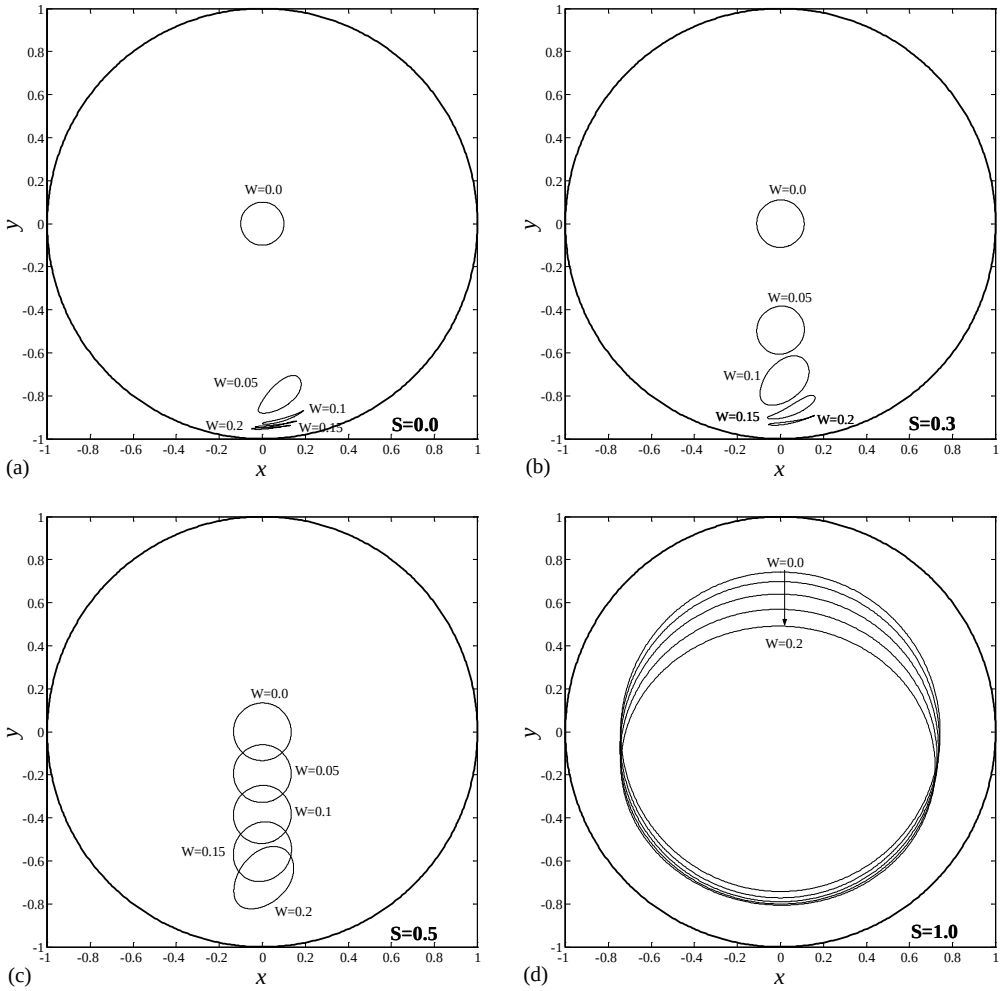

Fig. 8. Effect of gravity parameter (W) on the rotor whirl orbit response for bearing parameter (B) of 0.015, unbalance parameter (U) of 0.1 and spring parameter (S) of (a) 0.0; (b) 0.3; (c) 0.5; (d) 1.0.

a static operating position close to the clearance limit of the damper. As the spring parameter (S) is increased, the whirl center approaches the center of the damper. At value of $S = 1.0$, the rotor whirls in a circular orbit about the damper center. The whirl orbit for S values of 0.0 and 0.1 are very similar in position and magnitude supporting the earlier observation of the similarity in their dynamic behavior shown in Fig. 6.

The effects of the gravity parameter (W) on the rotor whirl orbit for various values of spring parameter (S) are illustrated in Fig. 8. For all the cases shown, the values of B and U are 0.015 and 0.1, respectively. As expected, the static operating position of the whirl orbit moves toward the damper's clearance circle limit as W is increased. It is further shown that for low values of S, the orbit approaches the clearance limit for cases of W of 0.15 and 0.2. The shape of the orbit indicates that the motion in the Y-direction was smaller compared to that in the X-direction. This is due to the higher stiffness of the oil-film when the clearance is smaller. In contrast, for $S = 0.5$, the orbits are almost circular although the static operating position is still offset from the damper's center. The magnitude of the offset decreases significantly for the case of $S = 1.0$.

3.5. *Bifurcations of the rotor response for values of* $B = 0.015$, $W = 0.05$ *and* $S = 0.3$

With the object to undertake a comprehensive bifurcation analysis of the rotor system, we consider the period-1 solution branches shown in Fig. 6(b), which represents B and W values of 0.015 and 0.05, respectively. Numerical continuation of the period-doubling bifurcation points on the solution branches representing a S value of 0.3 is further

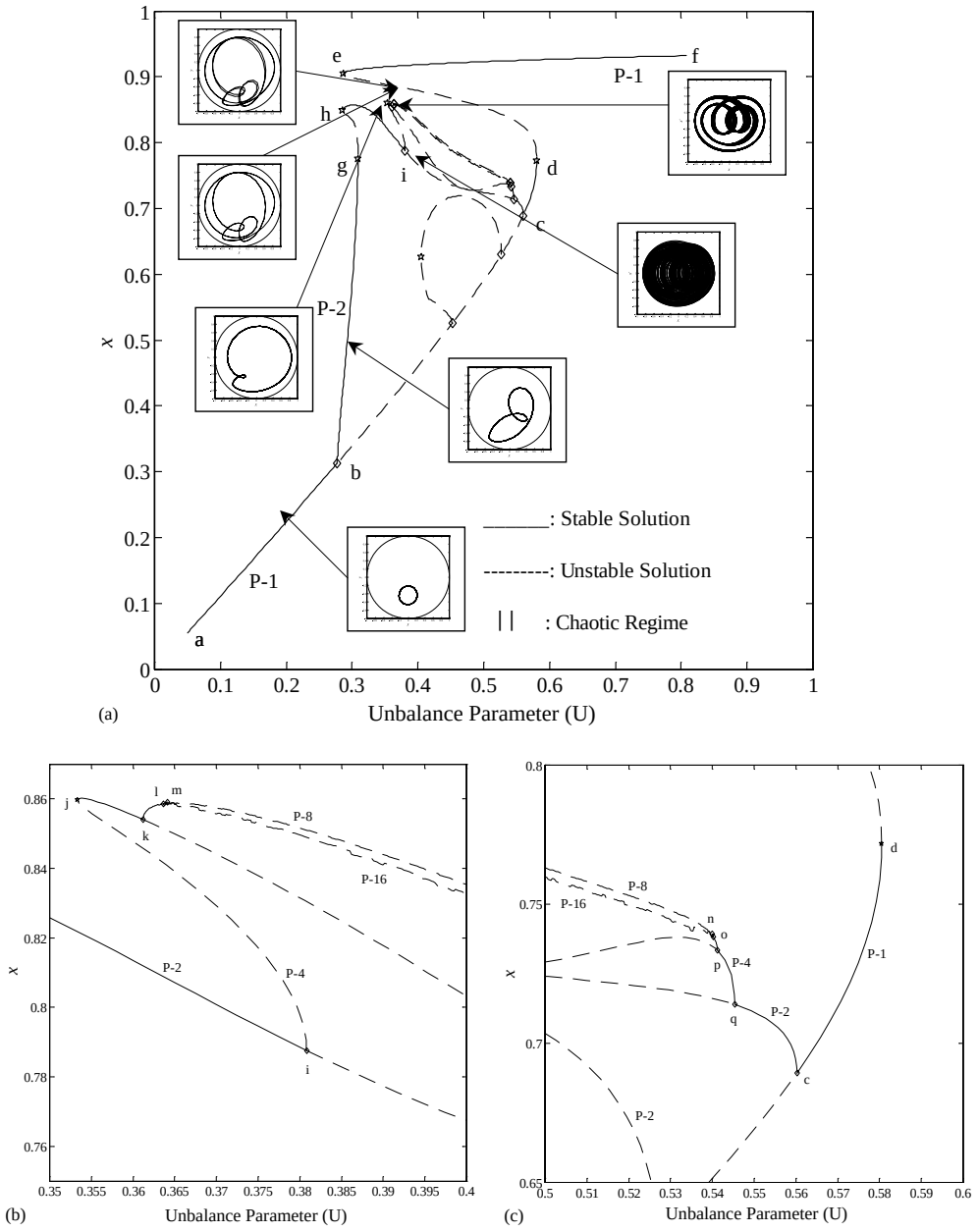

Fig. 9. (a) Bifurcation diagram of the rotor in squeeze-film dampers for values of bearing parameter (B) of 0.015, gravity parameter (W) of 0.05 and spring parameter (S) of 0.3; (b) enlargement of Fig. 9(a) for U values between 0.35 and 0.4; (c) enlargement of Fig. 9(a) for U values between 0.5 and 0.6. Bifurcations are: ☆ saddle-node; ◇ period-doubling.

undertaken in order to determine their entire dynamic behavior. The bifurcations of the response for $S=0.1$ have previously been confirmed to be similar to that of a rotor in dampers without centering springs. The authors previously undertook an in-depth study on the bifurcations of the response of a rigid rotor in dampers without centering springs (Inayat-Hussain et al., 2000). Some relevant results of this study are reproduced here for comparison purposes. For S values of 0.5 and 0.7, the bifurcations of the rotor response, which exhibited jump phenomena, are similar to that of a perfectly centered rigid rotor in dampers with centering springs. This case, where the rotor whirls in a circular orbit centered in the damper, has been thoroughly investigated, and therefore is not considered in this study (Mohan and Hahn, 1974; Taylor and Kumar, 1980; Li and Taylor, 1987).

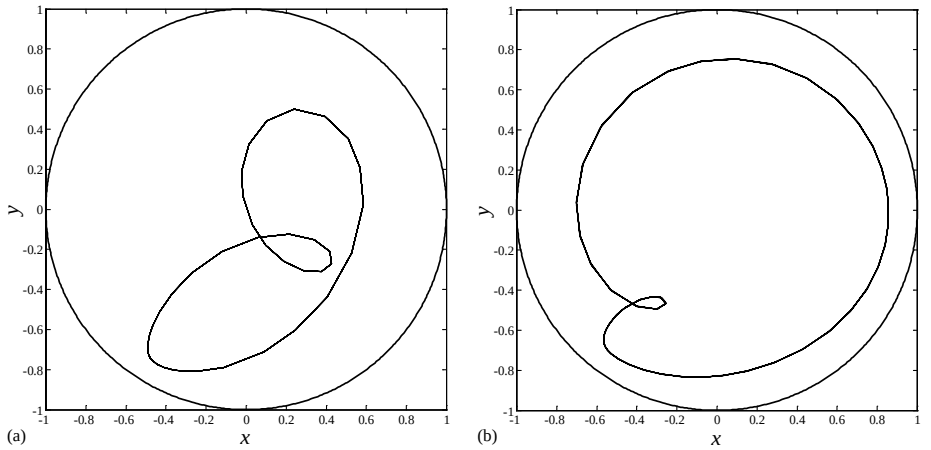

Fig. 10. Multiple period-2 attractors for values of bearing parameter (B) of 0.015, gravity parameter (W) of 0.05, spring parameter (S) of 0.3 and unbalance parameter (U) of 0.3. Initial conditions (a) $x(0) = 0.1$, $y(0) = -0.1$; (b) $x(0) = 0.1$, $y(0) = -0.25$.

The bifurcation diagram for $S = 0.3$ is shown in Fig. 9. The original solution branch of period-1, shown as curve a–f in Fig. 9(a), is observed to lose its stability via period-doubling and saddle-node bifurcations as the unbalance parameter (U) is varied from 0.05 to 0.8. The first period-doubling bifurcation point where the period-1 solution becomes unstable occurs at a U value of 0.2774, labeled 'b' in Fig. 9(a). At this point, a branch switching is undertaken to trace out a stable period-2 solution branch. Instead of directly going through yet another period-doubling bifurcation as would be expected in nonlinear dynamical system with asymmetric restoring forces, the stable period-2 solution branch is, however, observed to lose its stability through a saddle node bifurcation. The saddle-node bifurcation resulted in multiple period-2 attractors coexisting in the range of U between 0.2857 and 0.3088, respectively labeled 'g' and 'h' in Fig. 9(a). These attractors are shown in Fig. 10 for $U = 0.3$ and initial conditions $(x(0), y(0))$ of (0.1, −0.1) and (0.1, −0.25). The occurrence of jump phenomena associated with a period-1 orbit resulting in the coexistence of multiple period-1 orbits is not uncommon in the response of a rigid rotor in squeeze-film dampers with centering spring, as evident from Figs. 5 and 6, and several available publications (Mohan and Hahn, 1974; Taylor and Kumar, 1980; Zeidan and Vance, 1990). To the authors' knowledge, the occurrence of jump phenomena associated with the period-2 orbit in squeeze-film damper supported rotors has, however, never been previously reported in the available literature.

The stable period-2 solution branch emanating from the saddle-node bifurcation point labeled 'h' in Fig. 9(a) eventually loses its stability through a period-doubling bifurcation at $U = 0.3808$, label 'i', thus ensuring the continuation of the period-doubling sequence. Branch switching at point 'i' results in an unstable period-4 solution branch as indicated in Fig. 9(b), which shows an enlargement of Fig. 9(a) for U values between 0.35 and 0.4. The unstable period-4 becomes stable through a saddle-node bifurcation at a U value of 0.3533, shown as label 'j' in Fig. 9(b), before undergoing a period-doubling bifurcation at $U = 0.3612$, label 'k'. The bifurcation point 'i' is of the inverse period-doubling type as opposed to the regular period-doubling bifurcation that occurs at 'b' and 'k'. An inverse period-doubling bifurcation occurs when an unstable periodic orbit collapses into a stable periodic orbit of half its period and the two are replaced by an unstable periodic orbit of the lower period (Ott, 1993). The stable period-8 solution branch emanating from the point labeled 'k' is observed to undergo another period-doubling bifurcation at $U = 0.3636$, labeled 'l' in Fig. 9(b). Branch switching at this point revealed a stable period-16 orbit, which is also observed to undergo another period-doubling bifurcation at $U = 0.3641$, label 'm'. Attempts to continue branch switching beyond this point was however unsuccessful, indicating the possible existence of aperiodic motion.

All the unstable solution branches of period-16, 8, 4 and 2, which resulted from the sequence of period-doubling bifurcations, are shown in Fig. 9(c) to undergo a sequence of reverse period-doubling bifurcations. The unstable period-16, 8, 4 and 2 orbits become stable through these bifurcations at respective U values of 0.5400, label 'n'; 0.5402, label 'o'; 0.5412, label 'p'; and 0.5454, label 'q'. The stable period-2 solution branch eventually joins the original period-1 solution branch at $U = 0.5602$, labeled 'c' in Fig. 9(c). The stable period-1 solution branch emanating from the point labeled 'c' is observed to undergo saddle-node bifurcations, denoted by ☆ at labels 'd' and 'e'. A stable period-1 orbit is found to exist between a U value of 0.2869, labeled 'e' in Fig. 9(a), and the maximum U value of 0.8 considered in this study.

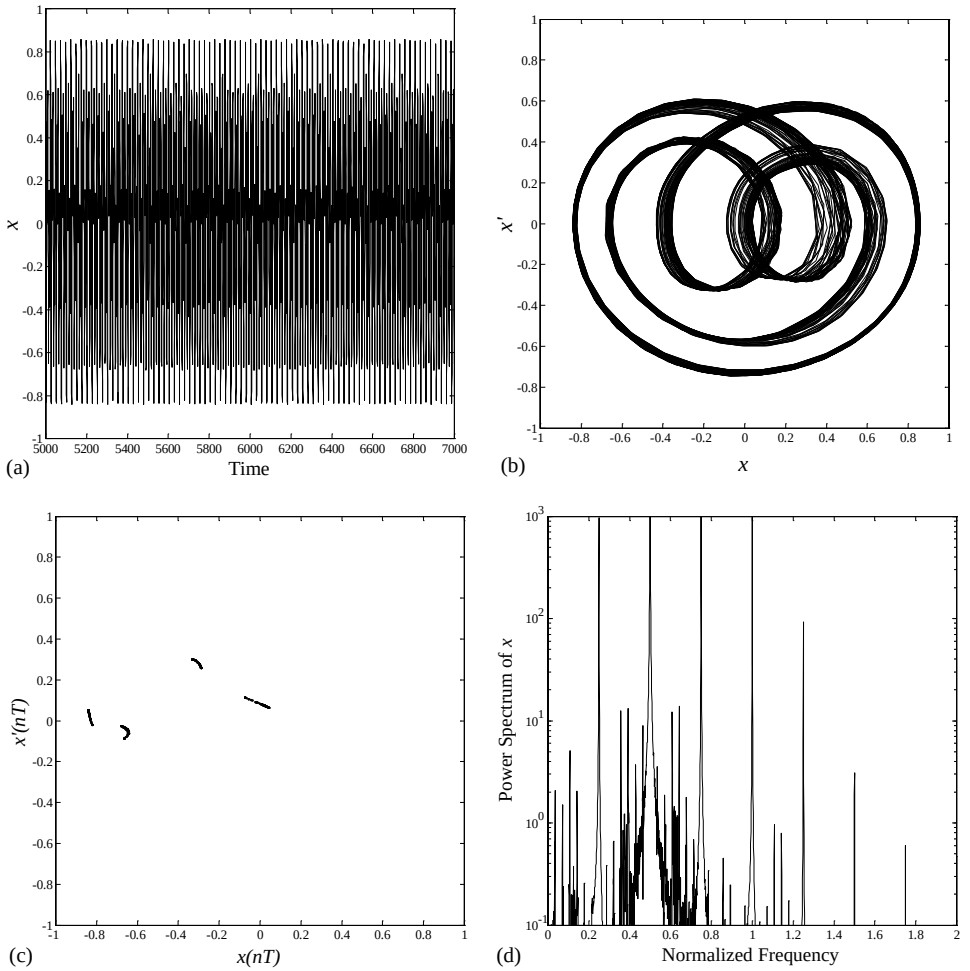

Fig. 11. Chaotic response of rotor for values of bearing parameter (B) of 0.015, gravity parameter (W) of 0.05, spring parameter (S) of 0.3 and unbalance parameter (U) = 0.365; (a) time series; (b) phase plane; (c) Poincaré map; (d) power spectrum.

Numerical integration of the equations of motion was undertaken for U values beyond the period-doubling point labeled 'm' in Fig. 9(b) where the branch switching failed to give any solutions. The results revealed the existence of chaotic motion for values of U from 0.365 to 0.367, and from 0.381 to 0.392. For $0.367 < U < 0.381$, orbits of period-1 and period-2 are found to coexist, whilst only the period-1 orbit is observed to exist for $U > 0.392$. The chaotic attractor in the range of U values from 0.365 to 0.367 differed significantly from the one that existed in the range $0.381 < U < 0.392$. The time series, phase plane, Poincaré map and power spectrum of the chaotic attractors for U values of 0.365 and 0.385 are respectively given in Figs. 11 and 12. The frequency of the power spectra shown in Figs. 11(d) and 12(d) is normalized by the driving frequency. The transition to chaotic motion, which exists in the range $0.365 < U < 0.367$, is via the period-doubling cascade route. The U values at the period-doubling bifurcation points shown in Fig. 9 were used to determine the Feigenbaum ratio. The ratio was found to converge to 4.759, in close agreement with the Feigenbaum constant of 4.669. On the other hand, the time series of the chaotic attractor shown in Fig. 12, representative of U values from 0.381 to 0.392, strongly suggests that the transition to chaos is via the intermittency route. The intermittency is due to the inverse period-doubling bifurcation, also known as type 3 intermittency, which occurs when an unstable periodic orbit collapses into a stable periodic orbit of half its period and the two are replaced by an unstable periodic orbit of the lower period (Ott, 1993). Referring to Fig. 9(b), it is clear that at $U = 0.3808$, label 'i', the unstable period-4 orbit collapses into the stable period-2 orbit resulting in an unstable period-2 orbit beyond this value of U.

The correlation dimension (D_{GP}), which was defined by Grassberger and Procaccia (1983) is used in this study. The correlation dimension is estimated from the slope of the plot that represents log ($C(l)$) versus log (l). $C(l)$ is the

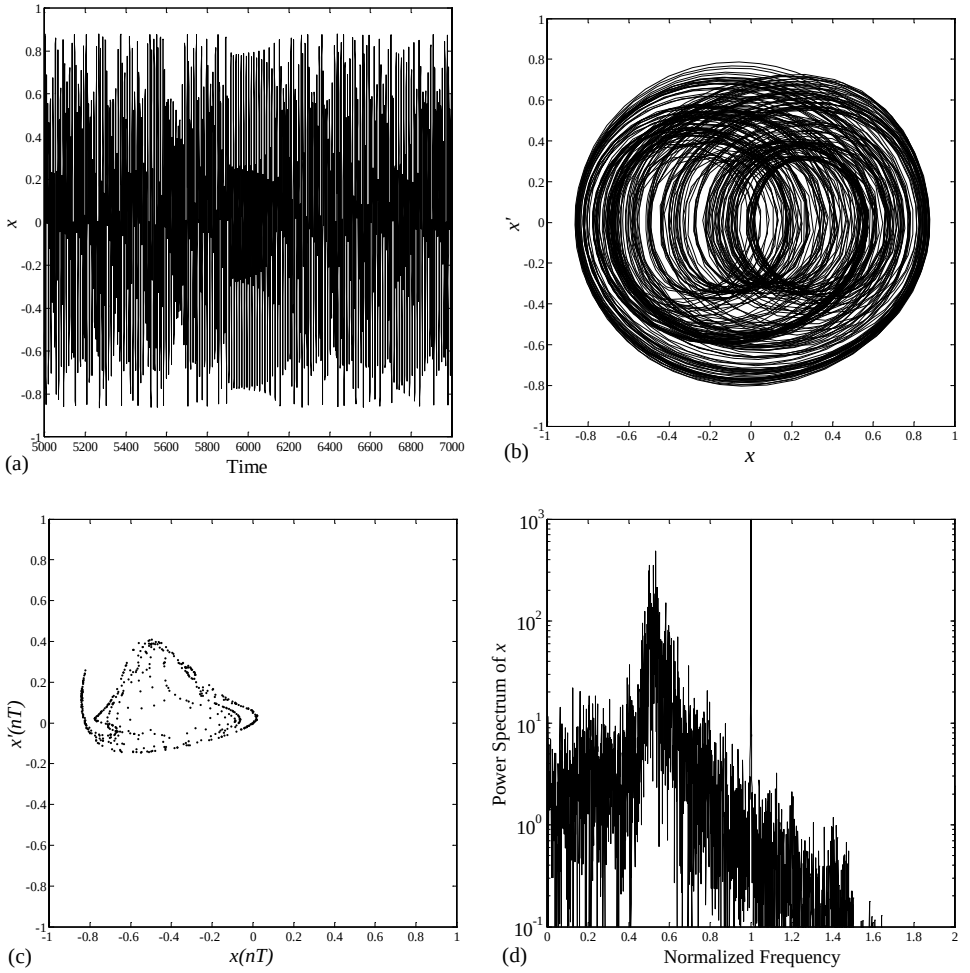

Fig. 12. Chaotic response of rotor for values of bearing parameter (B) of 0.015, gravity parameter (W) of 0.05, spring parameter (S) of 0.3 and unbalance parameter (U) = 0.385; (a) time series; (b) phase plane; (c) Poincaré map; (d) power spectrum.

correlation integral and is expressed as

$$C(l) = \lim_{N\to\infty}\left[\frac{1}{N^2}\sum_{i=1}^{N}\sum_{j=1}^{N} H(l - |\tilde{x}_i - \tilde{x}_j|)\right], \tag{19}$$

where the various quantities in Eq. (19) are: $\tilde{x}$ discrete points on the trajectory, N number of data-points $\tilde{x}_i$, l radius of n-dimensional hypersphere to test the system, H Heaviside function, i.e.

$$H(s) = \begin{cases} 1 \text{ if } s \geqslant 0 \\ 0 \text{ if } s < 0 \end{cases}.$$

The correlation dimension of the chaotic attractors at U values of 0.365 and 0.385, computed based on the Grassberger and Procaccia (1983) method, was respectively found to be 1.79 and 2.39, Fig. 13. Besides giving an indication of the degree of 'complexity' of the (chaotic) response, the correlation dimension (D_{GP}) gives an estimate of the number of degrees of freedom (N_f) needed to model the system dynamics. It can be shown (Mane, 1981) that N_f is related to D_{GP} by $D_{GP} \leqslant 2N_f \leqslant 2(D_{GP} + 1)$.

Some pertinent results from an earlier study on the bifurcations of a rigid rotor in squeeze-film damper without centering springs, the case of $S = 0$, are reproduced in Fig. 14 (Inayat-Hussain et al., 2000). Fig. 14(a) represents the superposition of solution branches emanating from a period-3 orbit, Fig. 14(c), on that emanating from a period-1

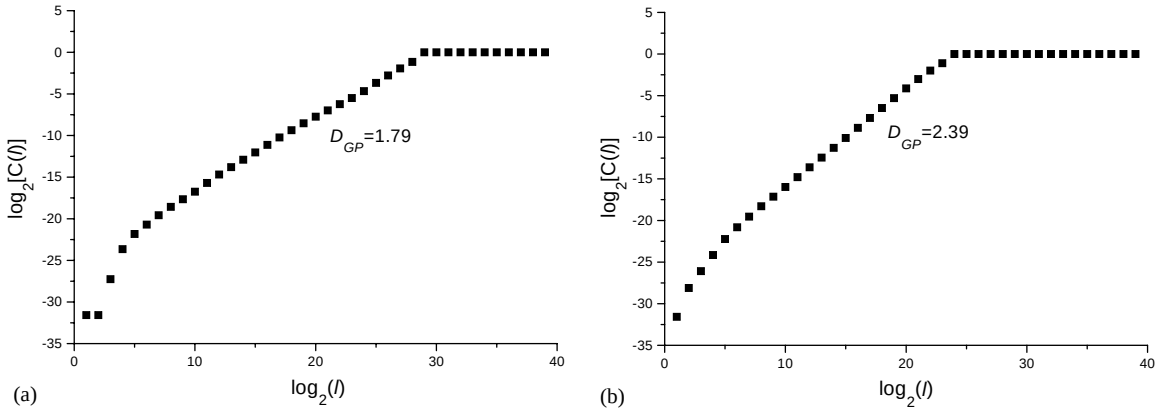

Fig. 13. Correlation integral corresponding to chaotic response of rotor for values of bearing parameter (B) of 0.015, gravity parameter (W) of 0.05 and spring parameter (S) of 0.3; (a) unbalance parameter (U) = 0.365; (b) unbalance parameter (U) = 0.385.

orbit, Fig. 14(b). Three regimes of chaotic motion were determined. The route to chaos in the first regime, which existed in the range $0.226 < U < 0.234$, is attributed to a sequence of period-doubling bifurcations of the period-1 orbit. The period-1 solution branch, shown in Fig. 14(b), is observed to sequentially bifurcate to period-2, 4, 8 and 16 orbits prior to the chaotic motion. A period-3 orbit, born from a saddle-node bifurcation, is found to coexist with the chaotic attractor. The period-3 orbit is also observed to undergo a sequence of period-doubling bifurcations resulting in chaotic motion in a range of U values between 0.264 and 0.282. The period-3 solution branch given in Fig. 14(c) is shown to bifurcate to period-6 and 12 orbits before chaotic motion sets in. The third regime of chaotic motion, which occurred immediately after the disappearance of the period-3 orbit due to a saddle-node bifurcation at $U = 0.3446$, is found to coexist with a period-4 orbit in the range of U between 0.345 and 0.36. The appearance of the chaotic attractor is attributed to a possible boundary crisis. A boundary crisis is a sudden destruction (or birth) of a chaotic attractor and its basin of attraction as a parameter is varied. An internal crisis, on the other hand causes a sudden change in the size of the chaotic attractor (Grebogi et al., 1983; Ott, 1993). Crises are associated with the collision of a chaotic attractor with a coexisting unstable periodic orbit or fixed point. The period-4 attractor, on the other hand, underwent a sequence of reverse period-doubling bifurcations resulting in a large amplitude period-1 orbit at higher values of U. The coexistence of the chaotic and period-3 attractors, for U value of 0.23, is illustrated in the phase-plane diagram and the Poincaré map shown in Fig. 15.

Comparison of the rotor response bifurcations in dampers without centering springs, $S = 0$, with dampers in centering springs, $S = 0.3$, revealed several distinctions. The most important observation is the nonexistence of the period-3 solution branch for the case of $S = 0.3$. The period-3 orbit that is observed in the case of the dampers without centering springs is not a generic bifurcation of the period-1 orbit, in the sense that it did not come into existence because the period-1 orbit lost its stability. It appeared and disappeared through a pair of saddle-node bifurcations. The period-3 orbit was in fact determined from the numerical integration of the equations of motion undertaken for various initial condition values. For the case of $S = 0.3$, the period-3 orbit was, however, not detected although similar initial condition values were used in the numerical integration scheme. This seems to suggest that the incorporation of the centering springs may have either caused the basin boundary of the period-3 attractor to shift, or to totally vanish. This was later confirmed by performing a two-parameter continuation from the saddle-node bifurcation point corresponding to $B = 0.015$, $W = 0.05$ and $U = 0.2013$, labeled 'a' on the period-3 solution branch in Fig. 14(c). Parameters U and S were simultaneously varied, and the parameter plane, which represent the plot of the values of S against U is shown in Fig. 16(a). The region below the curve corresponds to combination values of U and S where the period-3 solution occurs, whilst the region above the curve corresponds to combination values of U and S where the period-3 solution does not occur. It is evident that the period-3 solution does not exist for $S = 0.3$. Fig. 16(b), which represents the parameter plane resulting from the two-parameter continuation by simultaneously varying parameters W and S, further confirms that the period-3 solution does not exist for $S = 0.3$. Zhao and Hahn (1993) have reported on the existence of period-3 and period-6 motions in the response of a rigid rotor in eccentric squeeze-film dampers. The values of parameters used in their computation were, however, different from those used in this work. The continuous stability boundary in the $S - U$ and $S - W$ parameter spaces shown in Fig. 16 clearly shows the combination values of parameters where period-3 solution exists.

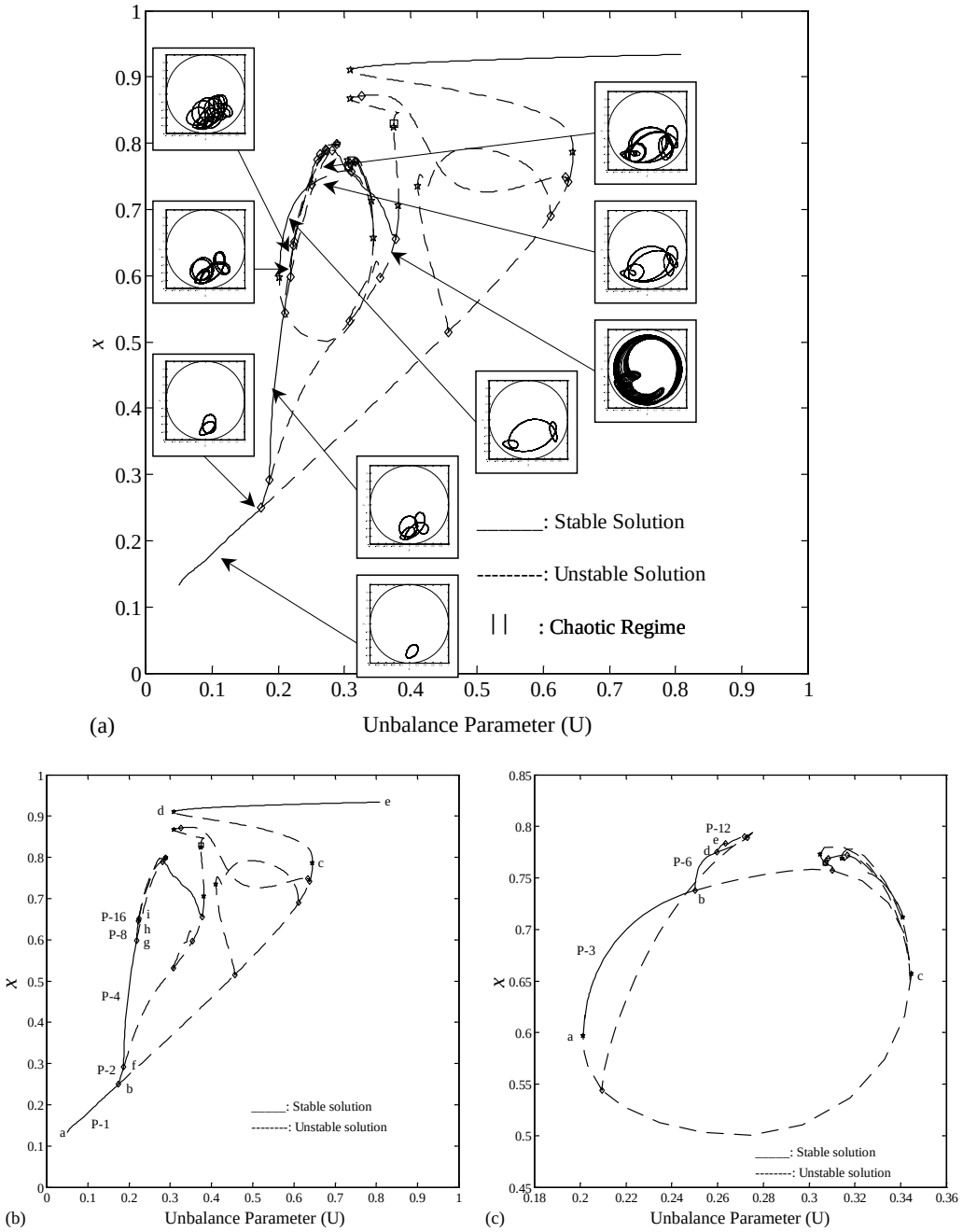

Fig. 14. (a) Bifurcation diagram of the rotor in squeeze-film dampers for values of bearing parameter (B) of 0.015, gravity parameter (W) of 0.05 and spring parameter (S) of 0.0; (b) branches emanating from period-1 solution; (c) branches emanating from period-3 solution. Bifurcations are: ☆ saddle-node; ◇ period-doubling; □ secondary Hopf.

The inverse period-doubling bifurcation that occurred for the case of dampers with S value of 0.3 is, however, not observed in the response of the dampers without centering springs. Whilst the common route to chaos in both cases of S are via a period-doubling cascade, the inverse period-doubling bifurcation that occurred in the case of $S = 0.3$ resulted in a type 3 intermittency transition to chaos. The boundary crisis route to chaos in the case of $S = 0$ is attributed to the period-3 solution branch. The rigid rotor in the dampers with centering springs, $S = 0.3$, is also found to bifurcate at a

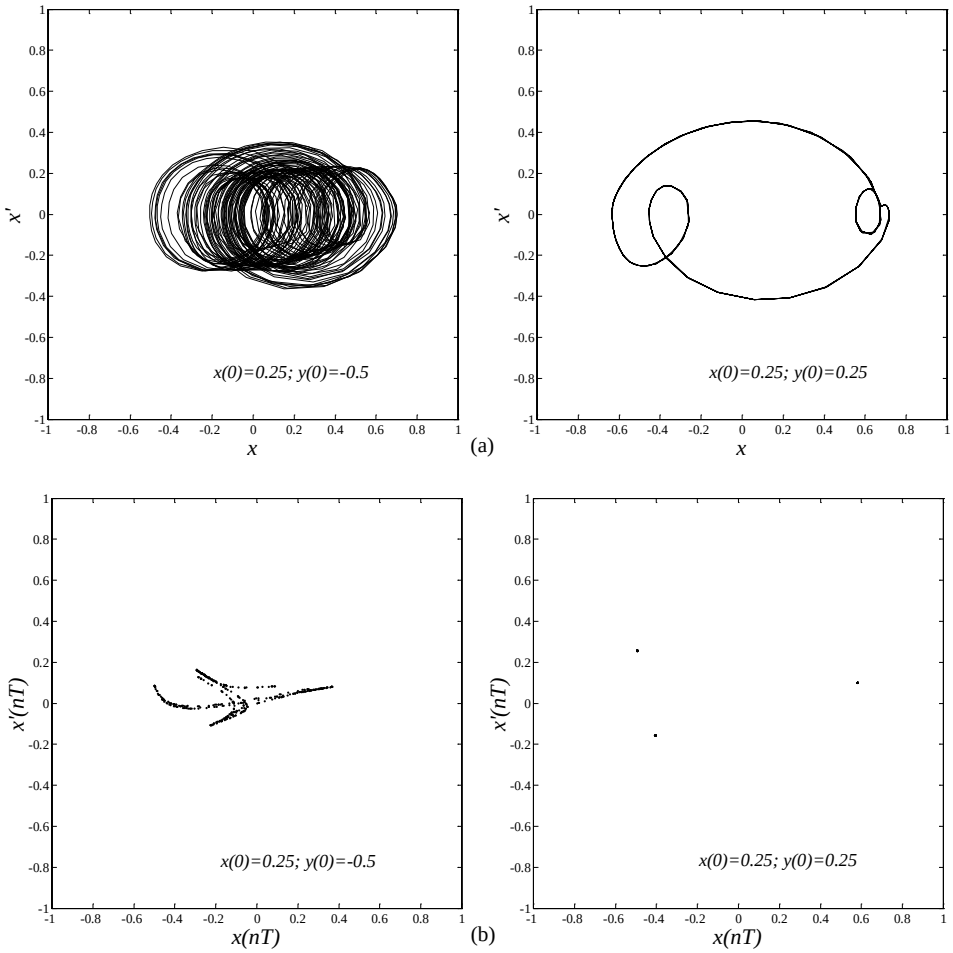

Fig. 15. Coexistence of chaotic and period-3 attractors for values of bearing parameter (B) of 0.015, gravity parameter (W) of 0.05, spring parameter (S) of 0.0 and unbalance parameter (U) of 0.23; (a) phase plane; (b) Poincaré map.

larger value of unbalance parameter (U), namely, $U = 0.2773$, in comparison with the case of dampers without centering springs, where the first bifurcation occurred at a U value of 0.1745. The centering springs therefore do not only serve to support and center the journal, but also increase the stability of the rotor system.

3.6. *Bifurcations in the response of rotors with similar values of static eccentricity ratio (Y_0)*

As an extension to the present investigation, we seek to determine if combination values of W and S resulting in the same static eccentricity position (Y_0) lead to similar bifurcation behavior. For this purpose, a value of $Y_0 = 0.5$ was selected. The combinations of W and S values that resulted in Y_0 value of 0.5 are respectively determined from Fig. 3 to be 0.05 and 0.3162; 0.1 and 0.4472; 0.15 and 0.5477; and 0.2 and 0.6325. The value of B is 0.015 and the value of U, selected as the bifurcation parameter, was varied from 0.05 to 0.8. The bifurcation diagram, shown in Fig. 17, revealed that the solution branches of the rotor response differed significantly. Although having similar values of Y_0 in all cases, the combination of the lowest W and S values, or in other words the lightest rotor in combination with the softest spring, appeared to be the most susceptible to response bifurcations. As the values of W and S increase, the susceptibility to bifurcations decreases. The response curves that represented the lower values of W and S, labeled 'A' and 'B' in Fig. 17, show the occurrence of period-doubling and saddle-node bifurcations. In addition, response curve 'B', which corresponds to $W = 0.1$, also showed the occurrence of a secondary Hopf bifurcation. The occurrence of saddle-nodes is observed in the response curves that represented the higher values of W and S, labeled 'C' and 'D' in Fig. 17. For the same value of unbalance parameter (U), it is evident from Fig. 17 that the vibration response amplitude

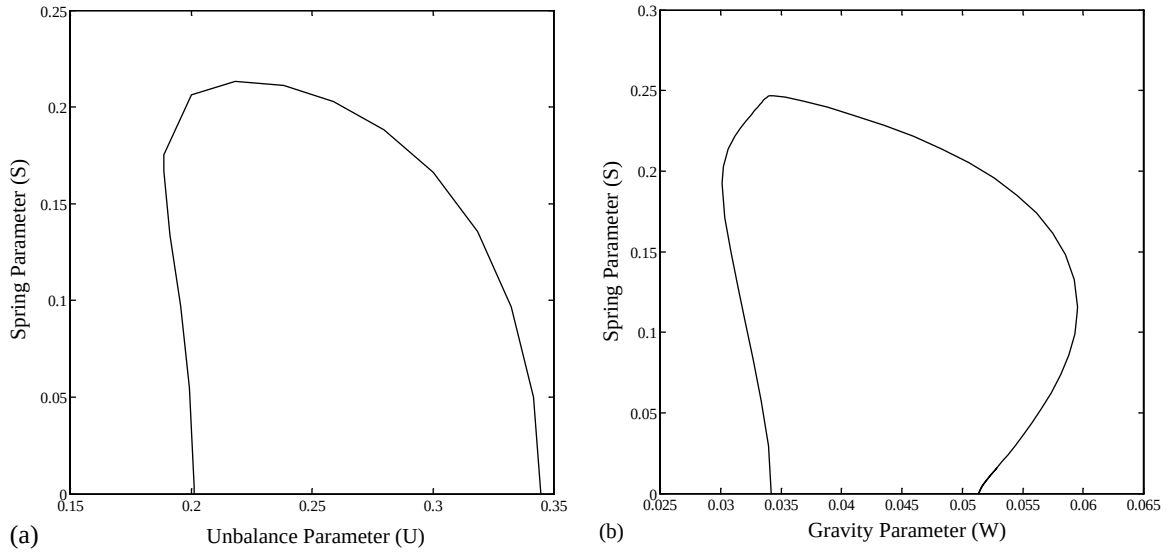

Fig. 16. Two parameter continuation of the period-3 solution corresponding to $B = 0.015$; (a) variation of U and S; (b) variation of W and S.

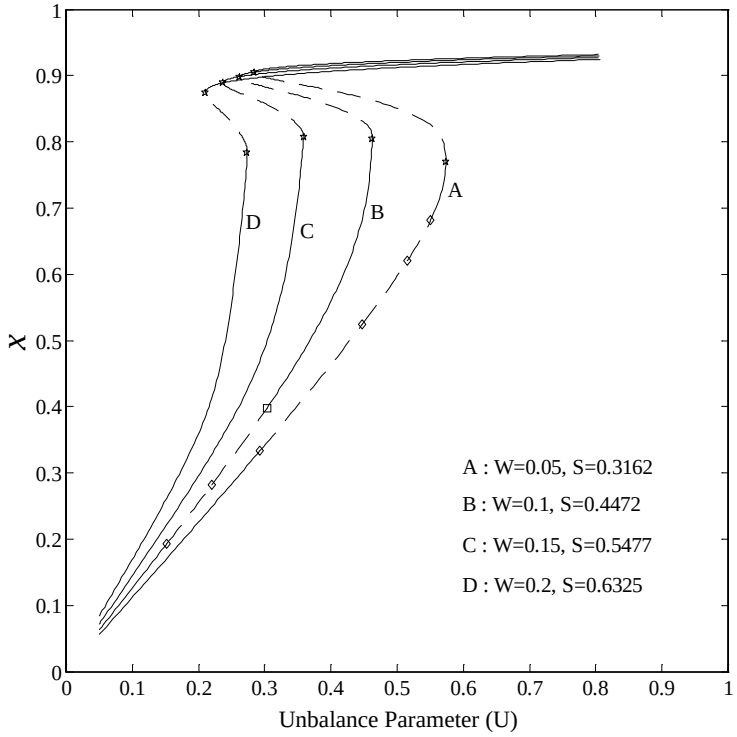

Fig. 17. Comparison of solution branches resulting from spring parameter (S) and gravity parameter (W) of different absolute values but with the same static eccentricity ratio (Y_0) value of 0.5. Value of bearing parameter (B) is 0.015. Bifurcations are: □ saddle-node; ○ period-doubling; γ secondary Hopf.

increases as the values of W and S increase. Rotor whirl orbits shown in Fig. 18 clearly illustrate the magnitude of the vibration response. The power spectrum and Poincaré map corresponding to the torus shown in Fig. 18(b) are given in Fig. 19. The Poincaré map, which shows a closed curve, is characteristic of quasi-periodic motion. The power spectrum

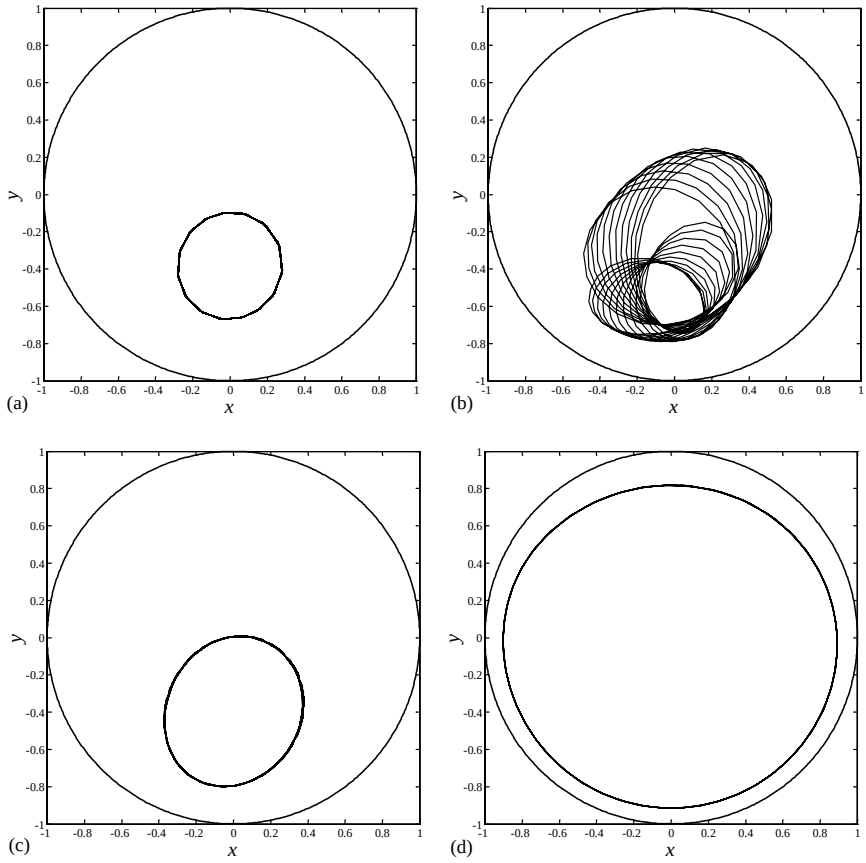

Fig. 18. Comparison of orbits for all solution branches in Fig. 14 for values of unbalance parameter (U) of 0.25, and initial conditions of $x(0) = 0.1$, $y(0) = -0.25$. (a) $W = 0.05$, $S = 0.3162$; (b) $W = 0.1$, $S = 0.4472$; (c) $W = 0.15$, $S = 0.5477$; (d) $W = 0.2$, $S = 0.6325$.

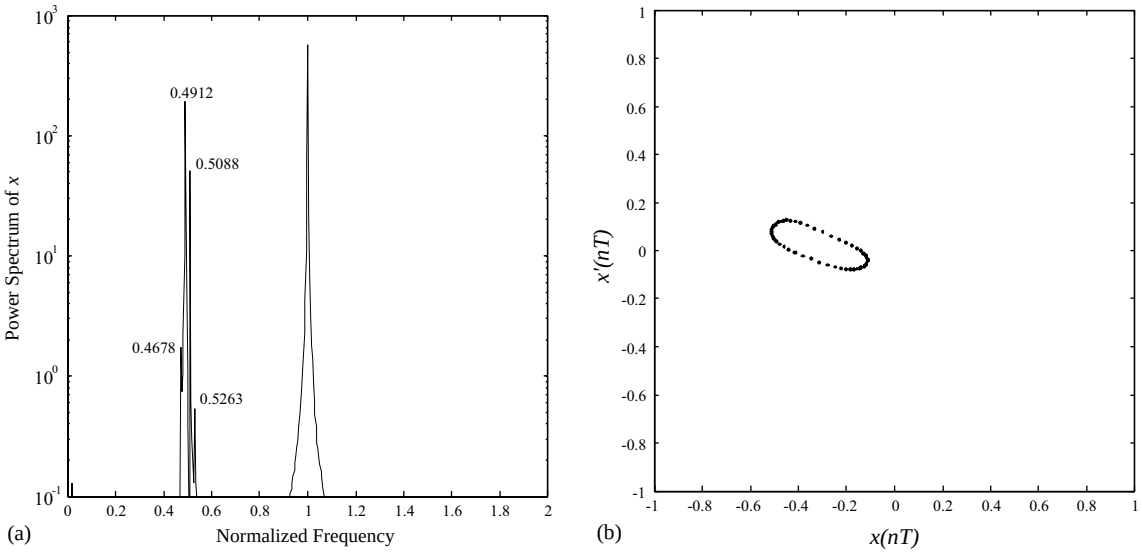

Fig. 19. (a) Power spectrum and (b) Poincaré map corresponding to the quasi-periodic rotor whirl orbit in Fig. 18(b).

further revealed a sub-synchronous frequency component accompanied by sidebands. The ratio of the frequency of the sub-synchronous motion to the forcing frequency was 0.4912……, an irrational number.

4. Concluding remarks

Nonlinear interactions between dynamic forces due to large rotor imbalance with fluid-film forces induced by cavitated squeeze-film dampers may limit the effectiveness of the dampers in controlling vibrations in rotating machinery. The bifurcations of the rotor response due to such interactions have been presented in this paper, with particular emphasis on the influence of design and operating parameters, namely the bearing (B), gravity (W), spring (S) and unbalance (U) parameters. Comparison of the rotor response bifurcations in dampers without centering springs, $S = 0$, with dampers fitted with centering springs, $S = 0.3$, revealed several distinct characteristics. For the case of the dampers without centering springs, the existence of a period-3 solution that formed a closed bifurcation curve consisting of a pair of saddle-nodes, was observed. This period-3 solution was, however, not observed in the case of dampers with centering springs, ($S = 0.3$). Period-doubling cascades of the period-1 and period-3 orbits, and boundary crisis were determined to be the routes to chaos for the case of the dampers without centering springs. In the presence of centering springs, the transitions to chaos were via the period-doubling and type 3 intermittency routes. While the period-doubling cascade appeared to be a common route to chaos in both cases, the type 3 intermittency transition to chaos, for the case of the dampers with centering springs, was due to an inverse period-doubling bifurcation of the period-2 solution branch. On the other hand, the boundary crisis route to chaos observed in the case of the dampers without centering springs was attributed to the period-3 solution branch. The incorporation of centering springs in squeeze-film dampers has been shown to decrease the rotor system susceptibility to bifurcation phenomena. This study further revealed that different combinations of W and S that result in the same static eccentricity ratio (Y_0) can exhibit remarkably different bifurcation behavior. From a practical point of view, the occurrence of nonsynchronous and chaotic motion in rotating machinery is undesirable and should be avoided as they introduce cyclic stresses in the rotor, which in turn may rapidly induce fatigue failure. The levels of rotor unbalance where nonsynchronous and chaotic motion were observed in this study, albeit being higher than the specified unbalance level for rotating machinery, may possibly occur with eroded rotors or in the event of a partial or an entire blade failure. Since most squeeze-film dampers in practical installations operate in a cavitated condition, one cannot de-emphasize the possible occurrence, in industrial rotating machinery, of the bifurcation phenomena arising from the interactions between large rotor imbalance forces and fluid-film forces as demonstrated in this work.

References

Booker, J.F., 1965. A table of the journal bearing integral. ASME Journal of Basic Engineering 87, 533–535.

Cookson, R.A., Kossa, S.S., 1979. The effectiveness of squeeze-film damper bearings supporting rigid rotors without a centralising spring. International Journal of Mechanical Sciences 21, 639–650.

Doedel, E.J., Keller, H.B., Kerneves, J.P., 1991a. Numerical analysis and control of bifurcation problems, Part 1. International Journal of Bifurcation and Chaos 1, 493–520.

Doedel, E.J., Keller, H.B., Kerneves, J.P., 1991b. Numerical analysis and control of bifurcation problems, Part 2. International Journal of Bifurcation and Chaos 1, 745–772.

Edney, S.L., Nicholas, J.C., 1999. Retrofitting a large steam turbine with a mechanically centered squeeze film damper. Proceedings of the 28th Turbomachinery Symposium, Turbomachinery Laboratory, Texas A&M University, pp. 29–40.

Grassberger, P., Procaccia, I., 1983. Measuring the strangeness of strange attractors. Physica D 9, 189–208.

Grebogi, C., Ott, E., Yorke, J.A., 1983. Crisis, sudden changes in chaotic attractors and transient chaos. Physica D 7, 181–200.

Gunter, E.J., Barrett, L.E., Allaire, P., 1977. Design of nonlinear squeeze-film dampers for aircraft engines. ASME Journal of Lubrication Technology 99, 57–64.

Holmes, R., 1972. The nonlinear performance of squeeze-film bearings. Journal of Mechanical Engineering Science 14, 74–77.

Holmes, R., Box, S., 1992. On the use of squeeze-film dampers in rotor support structures. Machine Vibration 1, 71–79.

Holmes, R., Dede, M., 1989. The vibration of an aero-engine rotor incorporating two squeeze-film dampers. Proceedings of the Institution of Mechanical Engineers, Part A: Journal of Power and Energy 203, 25–34.

Holmes, R., Dogan, M., 1982. Investigation of a rotor bearing assembly incorporating a squeeze-film damper bearing. Journal of Mechanical Engineering Science 24, 129–137.

Holmes, R., Sykes, J.E.H., 1996. Nonlinear phenomena in aero-engine rotor vibration. Proceedings of the Institution of Mechanical Engineers, Part G: Journal of Aerospace Engineering 210, 39–51.

Humes, B., Holmes, R., 1978. The role of sub-atmospheric film pressure in the vibration performance of squeeze-film bearings. Journal of Mechanical Engineering Science 20, 283–289.

Inayat-Hussain, J.I., 2001. A study on the dynamic performance of squeeze-film dampers. Ph.D. Dissertation, Graduate School of Science and Technology, Kobe University, Kobe, Japan.

Inayat-Hussain, J.I., Kanki, H., Mureithi, N. W., 2000. Bifurcation analysis of a rigid rotor in cavitated squeeze-film dampers. Proceedings of the First International Conference on Structural Stability and Dynamics, Taipei, Taiwan, December 7–9, 2000, pp. 333–338.

ISO 1940 (International Standards Organization), 1973. Balance quality of rotating rigid bodies. ISO Document 1940, Geneva, Switzerland.

Kanki, H., Kaneko, Y., Kurosawa, M., Yamamoto, T., 1998. Prevention of low-frequency vibration of high-capacity steam turbine units by squeeze-film damper. ASME Journal of Engineering for Gas Turbines and Power 120, 391–396.

Keller, H.B., 1991. Numerical Methods for Two-Point Boundary Value Problems. Dover, New York.

Leader, M.E., Whalen, J.K., Grey, G.G., Hess, T.D., 1995. The design and application of a squeeze-film damper bearing to a flexible steam turbine rotor. Proceedings of the 24th Turbomachinery Symposium, Turbomachinery Laboratory, Texas A&M University, pp. 49–57.

Li, X., Taylor, D.L., 1987. Nonsynchronous motion of squeeze film damper systems. ASME Journal of Tribology 109, 169–176.

Mane, R., 1981. On the dimension of the compact invariant sets of certain nonlinear maps. In: Rand, D.A., Young, L.S. (Eds.), Dynamical Systems and Turbulence. Springer Lecture Notes in Mathematics, Vol. 898, Springer, New York, pp. 230–242.

Mohan, S., Hahn, E.J., 1974. Design of squeeze film damper supports for rigid rotors. ASME Journal of Engineering for Industry 96, 976–982.

Ott, E., 1993. Chaos in Dynamical Systems. Cambridge University Press, Cambridge.

Seydel, R., 1988. From Equilibrium to Chaos—Practical Bifurcation and Stability Analysis. Elsevier, Amsterdam.

Szeri, A.Z. (Ed.), 1980. Tribology: Friction, Lubrication and Wear. McGraw-Hill, New York.

Taylor, D.L., Kumar, B.R.K., 1980. Nonlinear response of short squeeze film dampers. ASME Journal of Lubrication Technology 102, 51–58.

Zeidan, F., Vance, J.M., 1990. Cavitation and air entrainment effects on the response of squeeze-film supported rotors. ASME Journal of Tribology 112, 347–353.

Zhao, J.Y., Hahn, E.J., 1993. Subharmonic, quasi-periodic and chaotic motions of a rigid rotor supported by an eccentric squeeze film damper. Proceedings of the Institution of Mechanical Engineers, Part C: Journal of Mechanical Engineering Science 207, 383–392.

Zhao, J.Y., Linnett, I.W., Mclean, L.J., 1994. Subharmonic and quasi-periodic motions of an eccentric squeeze film damper-mounted rigid rotor. ASME Journal of Vibration and Acoustics 116, 357–363.